The Dynamics and Regulation of Actin Filaments in Vascular Endothelial Cells and in a Reconstituted Purified Protein System

by

Eric A. Osborn

B.S.E. Biomedical Engineering
Duke University, 1998

Submitted to the Department of Mechanical Engineering in Partial Fulfillment of the Requirements for the Degree of

Masters of Science in Mechanical Engineering

at the

Massachusetts Institute of Technology

February 2001

Signature of Author _____
Department of Mechanical Engineering
January 19, 2001

Certified by _____
C. Forbes Dewey, Jr.
Professor of Mechanical Engineering
Thesis Supervisor

Certified by _____
John H. Hartwig
Associate Professor of Cell Biology, Harvard Medical School
Thesis Supervisor

Accepted by _____
Ain Sonin
Chairman, Department Committee on Graduate Students

The Dynamics and Regulation of Actin Filaments in Vascular Endothelial Cells and in a Reconstituted Purified Protein System

by

Eric A. Osborn

Submitted to the Department of Mechanical Engineering on January 19, 2001 in Partial Fulfillment of the Requirements for the Degree of Master of Science in Mechanical Engineering

ABSTRACT

Cell motility and shape change are complex processes that depend primarily on the cytoplasmic dynamics and distribution of actin monomer and polymer. Proteins that regulate actin cycling control cellular architecture and movement. One method to measure parameters that characterize actin dynamics is photoactivation of fluorescence (PAF), which can simultaneously estimate the fraction of total actin polymerized (*PF*) and the lifetime of actin filaments (τ). By deciphering the relationships between actin dynamics and regulatory proteins, the complicated motions of cells and biological consequences of these movements can be better understood.

In purified actin solutions at steady-state, actin filament dynamics can be analyzed with PAF at long times following photoactivation. By increasing the width of the photoactivated band, actin filament turnover (τ ~ 8 hours) can be distinguished from actin filament diffusion. Proteins believed to stabilize actin filaments against depolymerization markedly slow actin filament turnover in wide photoactivated bands (τ ~ 65 hours). Decreasing the band width causes photoactivated fluorescence to decay more rapidly (τ ~ 3 hours) due to a combination of actin filament diffusion and turnover. Addition of actin-binding protein forms crosslinked actin gels that hinder filament diffusion and slow filament turnover (τ ~ 12 hours) in narrow photoactivated bands.

Endothelial cells decrease τ and *PF* in order to accelerate their migration speed, consistent with mechanisms attributed to ADF/cofilin *in vitro*. Removal of gelsolin in fibroblasts produces a similar correlation between motility, τ, and *PF*. Consistent with increased actin filament severing, fast-moving endothelial cells have an increased number of short actin filaments and more uncapped barbed ends, but paradoxically bind less cofilin. A mechanism of increasing endothelial cell motility is proposed that relies on actin filament severing to create uncapped pointed ends for ADF/cofilin-mediated depolymerization.

Thesis Supervisor: C. Forbes Dewey, Jr.
Title: Professor of Mechanical Engineering

Thesis Supervisor: John H. Hartwig
Title: Associate Professor of Cell Biology, Harvard Medical School

ACKNOWLEDGMENTS

I would like to thank my advisors, John H. Hartwig and C. Forbes Dewey, Jr. for their wonderful ideas, advice, and support throughout the process of shaping this research. I am also grateful for the continued mentorship and collaboration of James L. McGrath, who has immeasurably helped me focus and guide my thoughts about actin dynamics and cell movement. As well, I am indebted to the tireless effort of Sarah K. Chalos for her contributions to the studies with the purified protein system. Finally, I would like to thank the students and faculty of the Harvard–MIT Division of Health Sciences and Technology, a group with which I am grateful to be associated.

BIOGRAPHY

Eric Alan Osborn was born on October 2, 1975 in Battle Creek, MI to Larry and Margie Osborn. In 1994, Eric graduated from Port Huron Northern High School in Port Huron, MI and proceeded to attend college at Duke University in Durham, NC where he graduated in 1998 with a B.S.E. in Biomedical Engineering. In 1999, Eric began graduate study in the Department of Mechanical Engineering at MIT and the Medical Engineering/Medical Physics program at the Harvard–MIT Division of Health Sciences and Technology. Currently, he is continuing his doctoral research in this program at the Hematology Division of Brigham and Women's Hospital located in Boston, MA.

TABLE OF CONTENTS

LIST OF FIGURES

Description *Page*

Chapter I

Background and Literature Review

Despite the complexity of signals and proteins that are required to coordinate cellular movement, the final substrate is the protein actin, which coexists inside cells in both monomeric (G-actin) and filamentous (F-actin) states. Inside the cell, individual actin filaments are linked together to form a dense three-dimensional network called the actin cytoskeleton, which gives the cell shape and mechanical structure. Actin filaments are also highly dynamic, continuously adding and losing monomeric subunits from their ends in a process known as actin filament turnover. In order for cells to move, they must selectively break down and reassemble the actin cytoskeleton in specific cellular regions to produce coordinated extension and retraction of the leading edge, cell body, and tail. At the periphery of a crawling cell, membrane protrusion is driven by actin polymerization. At the cell interior in the bulk cytoskeleton, actin filaments are depolymerized to recycle actin monomers. At steady state, cells crawl by balanced actin polymerization and depolymerization in a cycle tightly regulated by a variety of actin-associated proteins. These include proteins that control the kinetics and access to actin filament ends, nucleate or sever actin filaments, sequester actin monomers, or alter actin monomer nucleotide exchange. Actin dynamics, structure, and regulation are important to a wide variety of normal and pathological situations because cells require an intact actin cytoskeleton and appropriate regulation of this structure for proper biological function. Since actin dynamics and cell movement are linked, understanding the relationships between actin dynamics and actin regulatory proteins provides insight into cell motility, morphology, and function.

Actin monomer

Actin is a globular 42 kDa protein [1] that has been highly conserved throughout evolution [2]. As one of the most abundant proteins in eukaryotic cells [3], actin is of

considerable biological significance due to its involvement in a large number of important cellular functions. There are six different isoforms of actin monomer known to exist in cells: α-cardiac, α-skeletal, α-vascular smooth muscle, β-non-muscle, γ-non-muscle, and γ-smooth muscle [4]. The actin isoforms are all ~ 375 amino acids in length and differ little from each other in sequence except near their amino terminus, which may confer isoform-specific actin-regulatory protein binding and filament assembly properties. The α- isoforms are found predominately in muscle cells, whereas the β- and γ- isoforms are predominant in non-muscle cells. However, each isoform may be expressed to varying degrees in spatially and temporally regulated patterns in many different cells [5].

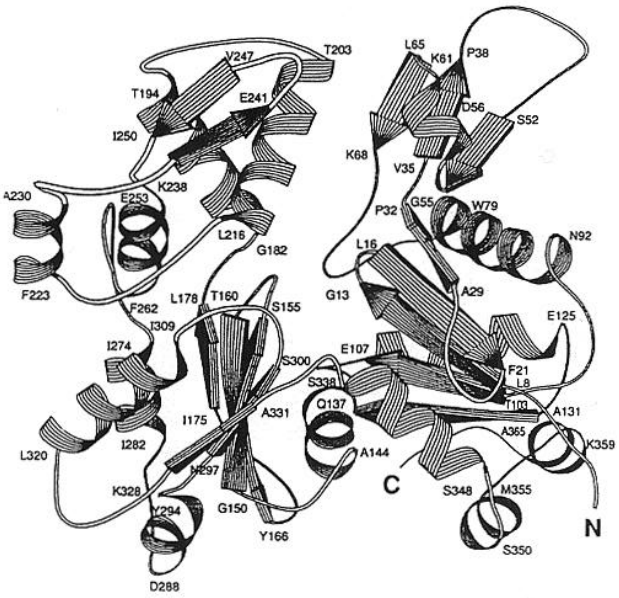

Fig. 1-1. *Atomic structure of the actin monomer*. The actin monomer is divided into two domains, separated by a nucleotide and divalent cation binding cleft (from Ref. [6]).

The structure of the actin monomer has been solved by x-ray crystallography [6]. An actin monomer is approximately of dimensions 5.5 nm × 5.5 nm × 3.5 nm and forms two domains, one small and one large, which are separated by a binding pocket that accepts a divalent cation and nucleotide (Fig. 1-1). Actin monomer has one high-affinity divalent cation (Ca^{2+} or Mg^{2+}) binding site and four low-affinity binding sites [7]. *In vivo*, the high-affinity site is thought to be bound to Mg^{2+}, since the polymerization kinetics are enhanced for Mg^{2+}-actin over Ca^{2+}-actin [8]. The conformation and properties of the actin monomer are different depending on whether Mg^{2+} or Ca^{2+} occupies this site [8, 9]. In addition, actin monomers bind one of

three nucleotide species: ATP, ADP•Pi, or ADP. The dynamics, protein binding affinities, structure, and regulation of actin are highly dependent on the nucleotide species composition of the actin monomer population.

Actin filaments

In the presence of physiological salts and pH, actin monomers spontaneously self-assemble into polymeric filaments. The self-assembly of actin filaments is a result of energetic considerations. Above a particular concentration, actin monomers disturb the disordered nature of water molecules enough to favor the entropic formation of actin filaments and restore water molecules to their native state. The concentration at which actin monomers will self-assemble under physiological conditions is known as the critical concentration, which, for ATP-actin, is $C_{c\text{-}ATP} \approx 0.1$ μM [10, 11]. Therefore, actin filament formation does not require the input of cellular energy (ATP) as long as the appropriate actin concentration and buffer conditions are met.

In purified actin solutions, polymerization begins with the formation of actin trimers, which serve as nucleation sites for further assembly of monomers [12]. Trimer formation is the rate-limiting step in polymerization, since the addition of actin filament seeds (pre-formed nucleation sites) eliminates the lag phase. Once actin trimers are created, rapid elongation occurs at the ends of the filament. The kinetics of filament elongation is strongly influenced by the nucleotide species bound to actin monomers [10, 13]. Eventually actin

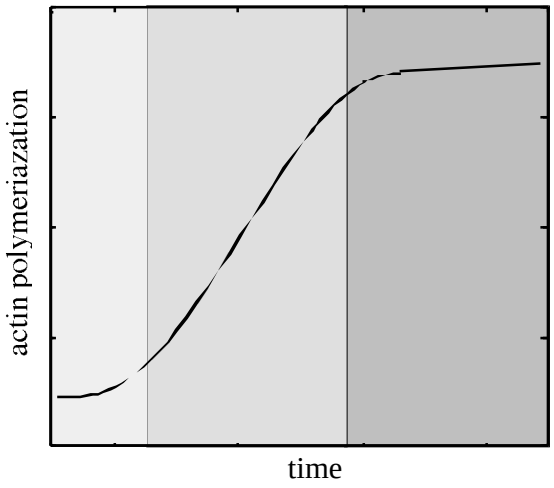

Fig. 1-2. *De novo actin polymerization.* The three shaded sections, from left to right, represent the lag, elongation, and steady state phases of actin filament formation.

filaments reach a steady state in which no net elongation of the existing filament population is observed (Fig. 1-2).

Actin filaments are helical polymers that are stabilized by multiple, noncovalent contacts between adjacent monomeric subunits. The actin filament structure can be described by either a one-start left-handed genetic helix of 5.9 nm pitch or a two-start right-handed helix of 72 nm pitch with a filament diameter of ~7 nm [14, 15]. Actin filaments are polarized: the two ends of the polymer can be differentiated both geometrically and biochemically. Filament ends are distinguished by their appearance in the electron microscope after labeling with myosin subfragment-1 (myosin-S1), a proteolytic fragment of heavy meromyosin. Actin filaments decorated in this manner exhibit a bipolar appearance in which the myosin-S1 groups align along the filament in a head-to-tail fashion, giving it an arrowhead appearance. In light of this observation, the ends of the actin filament are differentiated as ‘barbed’ and ‘pointed’. Biochemically, filament ends are distinct, and the rate constants for actin monomer assembly and disassembly bound to each nucleotide species must be considered independently.

Actin filament turnover

At long times *in vitro*, polymerized actin reaches a steady state in which there is no net change in actin filament lengths (Fig. 1-2). In the presence of excess ATP, due to different affinities for actin monomer at the barbed and pointed ends of the filament, actin filaments slowly elongate from the barbed end and shrink from the pointed end. The result is a net F-actin subunit flux from the barbed to pointed end [16], a mechanism known as turnover or treadmilling. Actin filament turnover is a cyclic process that relies on ATP hydrolysis to provide sufficient chemical energy to maintain the different filament end kinetics (Fig. 1-3) [10]. In the treadmilling model, actin monomers charged with ATP add to the barbed end where ATP-actin is hydrolyzed to an ADP•Pi-actin intermediate. Since actin is an ATPase, hydrolysis is accomplished intrinsically by actin filament subunits. ADP•Pi-actin is a stable intermediate state in actin filaments, but this

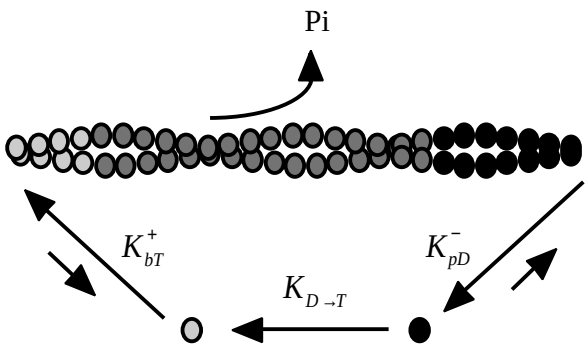

Fig. 1-3. *Actin filament treadmilling.* ATP-actin monomers (⭘) assemble at the barbed end, are hydrolyzed to ADP•Pi-actin (◍) as they flux through the actin filament, and dissasemble as ADP-actin (●) at the pointed end.

state slowly decays as Pi dissociates from the actin subunit while it cycles through the filament [17]. Therefore, as actin filament subunits approach the pointed end, they are predominately bound to ADP, an unstable state that favors F-actin subunit disassembly. Once depolymerized, free actin monomers exchange ADP for ATP to recharge their energy supply, thus completing the actin cycle.

The time required for an actin subunit to traverse a filament from barbed to pointed end defines the characteristic lifetime of the actin filament, also known as the actin filament turnover time (τ). This quantity is determined by the association and dissociation kinetics of actin monomers at the filament ends. Cellular actin filament turnover has been estimated from seconds to minutes, depending on the cell type and conditions [18-23]. However, *in vitro*, the actin filament lifetime is long (on the order of hours) because of the slow dissociation rate for monomers at the pointed end [24], and the absence of proteins that enhance filament dynamics.

Regulation of actin dynamics

Many different cytoplasmic proteins bind directly, or associate with factors that bind, to actin in order to influence actin dynamics. Actin-regulatory proteins have been studied in depth *in vitro* and are classified by their influence on the actin cycle. In general, these proteins control the availability of the ends of filaments to diffusing actin monomer, or directly influence the kinetics of monomer association, dissociation, and nucleotide

exchange. For simplicity, the actions of actin-associated proteins can be generalized into families of mechanisms: barbed and pointed end capping, acceleration of filament

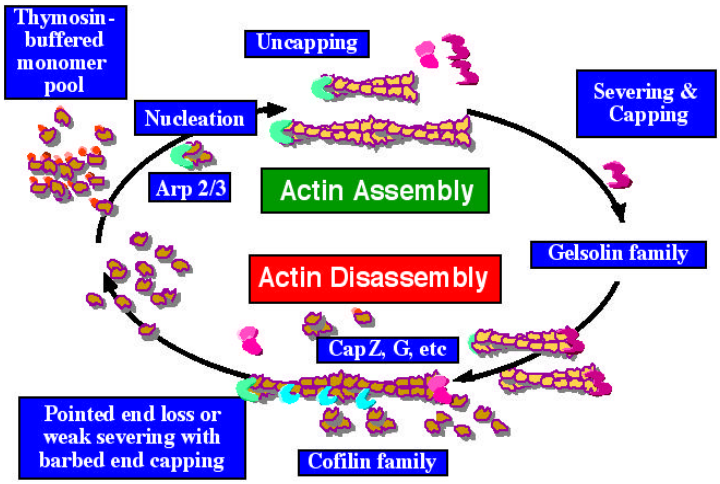

Fig. 1-4. *Regulation of actin dynamics.* Many different proteins affect the dynamics of actin as monomers and polymer. Protein mechanisms of action are highlighted in the text.

depolymerization filament severing and nucleation, nucleotide exchange enhancement, and monomer sequestration. The proteins and mechanisms currently thought to be of major importance in regulating and enhancing the actin cycle are shown in Fig. 1-4.

Many proteins, such as gelsolin and CapZ, bind to the barbed end of actin filaments, thus 'capping' this end and blocking actin monomer association. This greatly slows actin filament elongation and turnover, since the barbed end is the primary assembly site for actin monomers. Gelsolin binds tightly to the barbed end of actin filaments but is released by membrane polyphosphoinositides, a mechanism that promotes rapid actin filament polymerization [25, 26].

Pointed end capping in non-muscle cells occurs via actions of the Arp2/3 complex, which binds to this site with nM affinity [27], and tropomodulin [28]. Recently, however, the degree of pointed end capping achieved by the Arp2/3 complex has been questioned [29]. Due to the large excess of barbed end capping proteins, actin filaments that are additionally capped at pointed ends are likely to be extremely stable in cells, as this is the primary site of F-actin subunit disassembly.

Not only does the Arp2/3 complex bind to actin filament pointed ends, but it binds to the sides of pre-existing actin filaments and nucleates new filaments at 70° angles by associating with free actin monomers to form a barbed end polymerization site [27]. Nucleation by the Arp2/3 complex is activated by association with members of the

WASp family of proteins [30]. Due to its ability to form a barbed end nucleation site, the Arp2/3 complex has recently been implicated in numerous models of cell membrane protrusion involving dendritic actin networks [27, 31].

When barbed ends are capped, actin filament disassembly is slow, but it can be accelerated by actions of the ADF/cofilin protein family. ADF/cofilin binds to the sides of filaments, preferentially to ADP-actin subunits and, therefore, most likely near the pointed end, enhancing the kinetics of ADP-actin depolymerization ~25-fold *in vitro* [32]. Accelerated depolymerization by ADF/cofilin, in cooperation with barbed end capping, may be responsible for the high rates of actin filament turnover observed *in vivo* [33].

Actin filament severing is accomplished mainly by the gelsolin protein family, which, besides gelsolin, includes such proteins as adseverin, CapG, flightless, and villin [34]. In the presence of μM Ca^{2+} levels, gelsolin binds to the sides of actin filaments, severs them, and remains tightly associated with the newly formed barbed ends [35-37]. Therefore, gelsolin is a major response protein that affects both actin cytoskeletal architecture and dynamics in signaling cascades involving calcium by altering filament length and end exposure.

The intrinsic rate of nucleotide exchange on actin monomer can be accelerated in solution by proteins such as profilin. Profilin binds to free actin monomer in solution, exchanges ADP for ATP ~140x faster than monomer alone, and shuttles ATP-actin monomer to uncapped barbed ends [38, 39]. The intrinsic rate of nucleotide exchange by actin during rapid filament turnover may be limiting, and profilin provides a mechanism to overcome this barrier.

Monomer sequestering proteins, such as thymosin-β4, bind unpolymerized actin monomer at higher affinity than pointed actin filament ends, but not barbed ends [40]. Therefore, through sequestration, actin monomer concentrations can be held much higher

than the critical concentration *in vivo*, allowing discrete control of the availability of monomer for incorporation into filaments.

Recently the necessary components for reconstituting actin-based motility in the bacterial pathogens *Lysteria monocytogenes* and *Shigella* were discovered [41]. The required actin-binding proteins include the Arp2/3 complex, capping protein, and ADF/cofilin. However, the results of these experiments have been questioned by other investigators as possibly containing contaminating protein factors. Despite this progress, the reconstitution of actin dynamics with purified actin and regulatory proteins is currently unable to achieve the levels measured in cells. The reasons for this dichotomy between *in vitro* and *in vivo* characteristics of actin dynamics have yet to be determined.

The actin cytoskeleton

In cells, actin filaments are linked together to form a three-dimensional support structure that fills the cytoplasmic space. This dense meshwork of actin polymer and bound regulatory proteins is known as the actin cytoskeleton (Fig. 1-5). The actin cytoskeleton gives the cell shape, stiffness, and a mechanical scaffold that helps to fix the position of organelles and provides pathways for intracellular transport. The interfilament spacing of the cortical actin cytoskeleton has been modeled as an orthogonal lattice with a width of 20 to 100 nm [42, 43], through which the cell transports cytoplasmic solute and proteins.

The filamin protein family is responsible for creating the structure of the actin cytoskeleton in cells by binding two actin filaments and crosslinking them into a gel [44]. Filamin-A, expressed primarily in non-muscle cells, is also present in many diverse structures within the cell, such as broad lamellae in which filamin-A promotes the formation of orthogonal filament arrays [44, 45] and at the base of filopodia [46]. The importance of filamin-A in cytoskeletal organization and structure is evident in a natural line of human melanoma cells that lack this protein. Filamin-A-null cells crawl poorly via

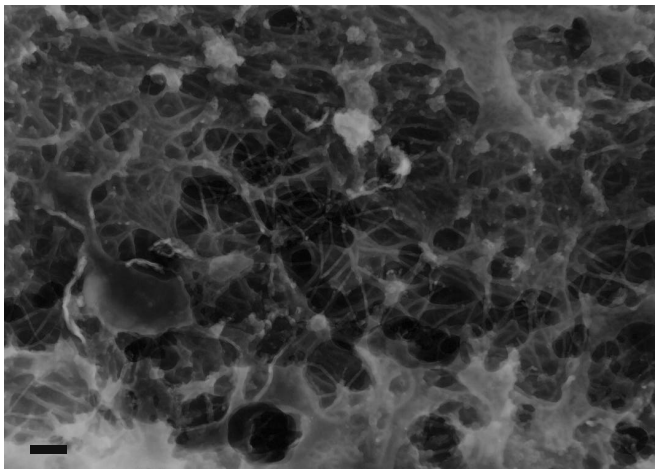

Fig. 1-5. *The actin cytoskeleton.* As typical for non-muscle cells, the endothelial cell actin cytoskeleton is a dense mesh of highly crosslinked actin filaments. Bar = 200 nm.

tubular projections and blebbing, while rescuing these cells with filamin-A cDNA results in a normal motile phenotype and the reappearance of lamellar protrusions and membrane ruffles [21, 47].

Dissolution of the actin cytoskeleton within a cell by decreased filament crosslinking and massive filament severing causes the cell cytoplasm to rapidly flow, known as a 'gel-sol' transition. An example of the rapid nature in which cells can change their physical state is the morphology of crawling neutrophils. In response to chemotactic signals, these cells move quickly across a substrate, constantly dissolving their internal network at the leading edge of the crawling cell and reforming this cell structure in the cell body [36, 48]. As in neutrophils and most other cells, the degree of crosslinking by filamin proteins is high [44]. There is some evidence that small actin filaments are able to diffuse through cytoskeletal pores [22] and are mobile near the plasma membrane [49]. In general, however, actin filaments are considered well anchored to each other in the cell cytoskeleton.

Cellular actin dynamics

In cells, the actin cytoskeleton is not simply a static structure, but one that must rapidly remodel when a cell changes shape or moves. Therefore, the bulk of cellular actin is dynamic via physical processes such as diffusion, turnover, severing, and nucleation. Tight spatial and temporal control of these dynamics is required to coordinate cell movement. When cells change shape, they recruit unpolymerized actin for assembly into

new or elongating filaments, and, at steady state, actin polymerization must be balanced by depolymerization elsewhere. Actin polymerized at the cell periphery in crawling cells is transported centripetally toward the cell body, implying that it is depolymerized in the bulk of the cytoskeleton [18-20, 50]. Therefore, cell movement and cytoskeletal actin remodeling are linked. A model of cell crawling involves actin polymerization and membrane protrusion at the leading edge, retrograde flow of F-actin to the cell interior, contraction of the cell body and tail, and depolymerization of actin filaments in the bulk, interior cytoplasm.

The lifetimes of actin filaments in cells are quite short as compared to purified actin solutions. Actin filament turnover is accelerated in cells due to the large number of regulatory proteins and signaling pathways that enhance actin dynamics. Fluorescence measurements in the lamellae of slowly moving fibroblasts [18] and highly motile keratocytes [19] provide estimates of actin filament lifetimes on the order of minutes and seconds, respectively, correlating actin filament turnover and the rate of cell movement. Because cellular actin is tightly regulated by numerous proteins and mechanisms, understanding the functions of these proteins provides the key to understanding how actin is remodeled in moving cells.

Development of fluorescence methods to measure actin dynamics

Actin dynamics can be measured in cells with variable precision. Two analogous fluorescence techniques offer the best estimates of parameters that describe the dynamic nature of cellular actin: photoactivation of fluorescence (PAF) and fluorescence recovery after photobleaching (FRAP). In PAF, a non-fluorescent, caged precursor actin molecule is uncaged by exposure to ultraviolet (UV) light in a small spot or rectangular region within the cell. FRAP is the inverse technique, in which the fluorescence of a labeled actin molecule is quenched with high-intensity light at the excitation wavelength of the fluorophore. Fluorescence decay or recovery is then measured in the subcellular photoactivated or photobleached area, respectively, and interpreted with mathematical

models that describe cellular actin transport. One theory relating labeled actin dynamics and photoactivated fluorescence decay is the Tardy Model, which computes of the mobility of actin monomer (D_m), the fraction of total actin polymerized (*PF*), and the actin filament turnover time (τ) [51]. The Tardy Model has been used to quantitate actin dynamics in various cell types such as endothelium, fibroblasts, and melanoma cells [21, 22], and the resulting measurements are consistent with those previously published by other investigators [18-20, 23].

Actin dynamics and movement in endothelial cells

Following mechanical wounding of confluent monolayers of endothelial cells and overnight recovery, distinct morphological and motile subpopulations of endothelial cells are observed in different regions with respect to the wound (Fig. 1-6) [21]. Wounding a confluent endothelial monolayer removes the inhibitory effects of intercellular contacts on cells near the wound, increasing cellular spacing, and activating the cell to crawl. In the undisturbed, confluent endothelial monolayer far away from the wound (zone 4), the cells retain the characteristic cobblestone morphology and low rate of movement expected for quiescent endothelial cells. Endothelium intermediate to the wound and the confluent region (zone 3) exhibits an elongated morphology perpendicular to the wound

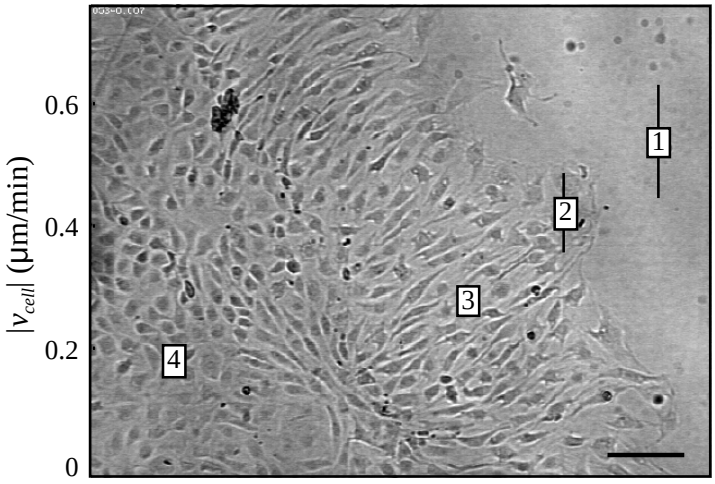

Fig. 1-6. *Endothelial cell speed correlates with morphological changes.* After overnight recovery from wounding, endothelial cells organize into distinct morphological zones: (1) subconfluent, (2) wound edge, (3) elongated, and (4) confluent. Average cell speed ($|v_{cell}|$) decreases with increased distance from the wound (from Ref. [21]). Bar = 100 μm.

edge and a faster rate of movement. At the wound edge (zone 2), endothelial cells remain in contact with the monolayer, but rapidly extend cellular processes into the wound, increase their speed, and assume a more spread morphology. The fastest moving endothelial cells are subconfluent or free from cellular contact in the wound (zone 1), and assume the phenotype of a typical motile cell with broad lamellipodia and filopodia extending from the leading edge.

Motile Zone	D_m ($\mu m^2/s$)	*PF*	τ (*min*)	$\lvert v_{cell} \rvert$ (μm/min)
1. Subconfluent	3.1 ± 0.4	0.36 ± 0.04	7.5 ± 2.0	0.53 ± 0.09
2. Wound Edge	3.3 ± 0.8	0.42 ± 0.08	11.7 ± 6.0	0.41 ± 0.06
3. Elongated	2.2 ± 0.6	0.57 ± 0.09	19.0 ± 6.4	0.28 ± 0.02
4. Confluent	2.3 ± 0.8	0.73 ± 0.11	38.9 ± 11.4	0.17 ± 0.01

Table 1-1. *Endothelial actin dynamics correlate with cell speed.* Monomer diffusion coefficient (D_m), polymer fraction (*PF*), filament turnover time (τ), and cell speed ($\lvert v_{cell} \rvert$) measured in the different motile zones from Fig. 1-6 (data from Ref. [21]).

In addition to morphological differences, root-mean-square (RMS) cell speed decreases with increasing distance from the wound (Fig. 1-6). PAF measurements of endothelial cell actin dynamics exhibit a positive correlation between cell speed, polymer fraction, and actin filament turnover (Table 1-1). The slowest moving (confluent) and fastest moving (subconfluent) endothelial cells differ in *PF* by ~50% and in τ by more than a factor of five. Thus, individual endothelial cells accelerate actin filament turnover and decrease the amount of polymerized actin in order to increase steady state motility [21].

Actin dynamics in subconfluent gelsolin knockout fibroblasts

Fibroblasts isolated from gelsolin knockout (G-) transgenic mice crawl poorly in comparison to wild-type cells (G+) [52]. This implies the importance of gelsolin, a potent actin filament severing and barbed end capping protein, in the coordination of normal

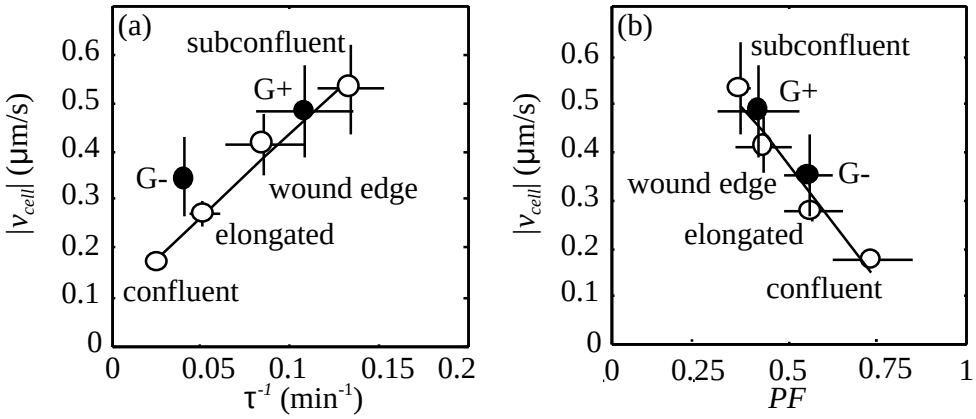

Fig. 1-7. *Actin dynamics in subconfluent fibroblasts* (●) *upon removal of gelsolin.* Gelsolin knockout fibroblasts (G-) crawl slower than wild-type (G+) and exhibit changes in actin dynamics consistent with measurements in the endothelial cell (○) motile zones from Fig. 1-6. (a) Actin filament turnover rates (τ^{-1}) markedly decrease in G- fibroblasts, coinciding with (b) an increase in the fraction of total actin polymerized (*PF*). (from Ref. [21])

cellular movement. The observed changes in motility between subconfluent G- and G+ fibroblasts are similar to the transition between motile phenotypes observed in wounded BAEC monolayers. PAF measurements reveal that the slower moving G- fibroblasts exhibit slower actin filament turnover ($\tau = 25.0 \pm 6.1$ min) and a greater fraction of actin polymerized (*PF* ~ 55 ± 7%) than the faster moving G+ phenotype ($\tau = 9.3 \pm 4.7$ min; *PF* ~ 41 ± 11%) [21]. The changes in actin dynamics that occur in subconfluent fibroblasts upon the removal of gelsolin show positive correlations with cell speed similar to measurements in endothelial cells (Fig. 1-7). This result indicates that the capping and severing activities of gelsolin are consistent with the mechanisms by which actin dynamics are regulated in endothelial cells [21].

The importance of actin dynamics and endothelial cells in physiology

Actin dynamics are integral to many normal and pathological processes in the body and are therefore essential to understanding physiology [53]. All animal cells crawl or change their shape throughout their lives, and these motile and structural changes are directly related to dynamic changes in the cellular actin cytoskeleton. Not only does the actin

architecture change in moving cells, but the ratio of actin monomer to polymer, the rate of actin filament turnover, the length of actin filaments, and the exposure of actin filament ends are all tightly regulated during these processes. In fetal development, there are numerous examples of cells altering their shape and motile state (e.g. gastrulation) as the embryo forms by patterned cellular differentiation and proliferation. Activation of blood platelets in the coagulation cascade following injury to the vascular wall is another example of the importance of actin dynamics in physiology: resting, discoid platelets circulating in the blood must rapidly alter their shape in order to reestablish the structure of a compromised blood vessel and facilitate vessel repair [54]. Blocking actin dynamics eliminates this important platelet function.

Endothelial cells, which line the inner surface of the vasculature, also depend on proper actin cytoskeletal structure and dynamics. Situated at the barrier between flowing blood and soft tissue, the endothelium senses fluid forces and extracellular chemical signals in the blood to regulate macromolecule permeability, maintain vascular tone, and provide a surface resistant to blood clot formation [55]. Damage to the endothelial lining promotes thrombotic episodes, potentially resulting in myocardial infarct and stroke. In response to vascular wounding and signals promoting new blood vessel formation such as angiogenesis, endothelial cells are stimulated to move, redefining and remodeling their actin cytoskeletons. The fraction of total cellular actin incorporated into filaments, the lifetime of these filaments, the structure of the actin cytoskeleton, and the linkages between actin and cell-substrate adhesion sites determine the cell's shape, stiffness, potential to crawl, and integrity of attachment to the artery wall, all of which affect endothelial function *in vivo*.

Goals of this thesis

The overall thrust of this research is to further understand the dynamics and regulation of the actin cytoskeleton by actin-associated proteins in the context of cellular shape change and motility. This is an ambitious undertaking, since the regulation of actin dynamics is

an extremely complex problem involving synergy between many different proteins. In order to narrow the scope of this research, from the many model systems for studying actin dynamics such as cellular extracts, bacterial pathogens *Lysteria monocytogenes* and *Shigella*, and every known cell type, this thesis will focus on examination and comparison of actin dynamics in a reconstituted purified protein system and in endothelial cells. Similarly, the focus on actin regulation is narrowed to make the problem tractable by investigating only a few specific actin-associated proteins believed to be important in actin cycling. Powerful fluorescence techniques are used to measure actin polymer fraction, diffusivity, and filament turnover. These methods are supplemented with classical biochemical techniques to analyze actin polymerization and protein levels in cells and purified solutions.

Chapters II and III of this thesis develop the theory and experimental results for a system to measure actin filament dynamics in purified actin solutions with PAF. This reconstituted purified protein system is novel in that it allows the direct observation of the dynamic processes at work via the fluorescence decay of labeled actin monomers. It also is the ideal system to noninvasively analyze actin filament dynamics at a true steady state, outside of the complex cellular environment. The ultimate aspirations of this work are to reconstitute a purified model of cellular actin architecture and dynamics *in vitro*, while learning more about the function of the actin regulatory proteins involved in cellular processes.

Actin dynamics and regulation in endothelial cells moving at different speeds are investigated in Chapter IV. When endothelial cells migrate from their normal resting state, they must change their speed, shape, and, therefore, actin dynamics. The mechanism that regulates this transition is unknown but is most likely related to the functions of known actin-associated proteins. By understanding how the state of actin changes and examining the distributions of certain actin-regulatory proteins, mechanisms of altering endothelial cell speed by these proteins can be determined.

REFERENCES

1. Elzinga M, Collins JH, Kuehl WM, Adelstein RS: Complete amino-acid sequence of actin of rabbit skeletal muscle. Proc Natl Acad Sci U S A 1973; 70(9): 2687-91.

2. Hightower RC, Meagher RB: The molecular evolution of actin. Genetics 1986; 114(1): 315-32.

3. Pollard TD: Actin. Curr Opin Cell Biol 1990; 2(1): 33-40.

4. Vandekerckhove J, Weber K: At least six different actins are expressed in a higher mammal: an analysis based on the amino acid sequence of the amino-terminal tryptic peptide. J Mol Biol 1978; 126(4): 783-802.

5. Herman IM: Actin isoforms. Curr Opin Cell Biol 1993; 5(1): 48-55.

6. Kabsch W, Mannherz HG, Suck D, Pai EF, Holmes KC: Atomic structure of the actin:DNase I complex. Nature 1990; 347(6288): 37-44.

7. Carlier MF, Pantaloni D, Korn ED: Fluorescence measurements of the binding of cations to high-affinity and low-affinity sites on ATP-G-actin. J Biol Chem 1986; 261(23): 10778-84.

8. Carlier MF, Pantaloni D, Korn ED: The effects of Mg2+ at the high-affinity and low-affinity sites on the polymerization of actin and associated ATP hydrolysis. J Biol Chem 1986; 261(23): 10785-92.

9. Frieden C, Lieberman D, Gilbert HR: A fluorescent probe for conformational changes in skeletal muscle G- actin. J Biol Chem 1980; 255(19): 8991-3.

10. Korn ED, Carlier MF, Pantaloni D: Actin polymerization and ATP hydrolysis. Science 1987; 238(4827): 638-44.

11. Bonder EM, Fishkind DJ, Mooseker MS: Direct measurement of critical concentrations and assembly rate constants at the two ends of an actin filament. Cell 1983; 34(2): 491-501.

12. Wegner A, Engel J: Kinetics of the cooperative association of actin to actin filaments. Biophys Chem 1975; 3(3): 215-25.

13. Pollard TD: Rate constants for the reactions of ATP- and ADP-actin with the ends of actin filaments. J Cell Biol 1986; 103(6 Pt 2): 2747-54.

14. Milligan RA, Whittaker M, Safer D: Molecular structure of F-actin and location of surface binding sites. Nature 1990; 348(6298): 217-21.

15. Amos LA: Structure of muscle filaments studied by electron microscopy. Annu Rev Biophys Biophys Chem 1985; 14: 291-313.

16. Wegner A: Head to tail polymerization of actin. J Mol Biol 1976; 108(1): 139-50.

17. Carlier MF, Pantaloni D: Direct evidence for ADP-Pi-F-actin as the major intermediate in ATP- actin polymerization. Rate of dissociation of Pi from actin filaments. Biochemistry 1986; 25(24): 7789-92.

18. Wang YL: Exchange of actin subunits at the leading edge of living fibroblasts: possible role of treadmilling. J Cell Biol 1985; 101(2): 597-602.

19. Theriot JA, Mitchison TJ: Actin microfilament dynamics in locomoting cells. Nature 1991; 352(6331): 126-31.

20. Theriot JA, Mitchison TJ: Comparison of actin and cell surface dynamics in motile fibroblasts. J Cell Biol 1992; 119(2): 367-77.

21. McGrath JL, Osborn EA, Tardy YS, Dewey CF, Jr., Hartwig JH: Regulation of the actin cycle in vivo by actin filament severing. Proc Natl Acad Sci U S A 2000; 97(12): 6532-6537.

22. McGrath JL, Tardy Y, Dewey CF, Jr., Meister JJ, Hartwig JH: Simultaneous measurements of actin filament turnover, filament fraction, and monomer diffusion in endothelial cells. Biophys J 1998; 75(4): 2070-8.

23. Kreis TE, Geiger B, Schlessinger J: Mobility of microinjected rhodamine actin within living chicken gizzard cells determined by fluorescence photobleaching recovery. Cell 1982; 29(3): 835-45.

24. Selve N, Wegner A: Rate of treadmilling of actin filaments in vitro. J Mol Biol 1986; 187(4): 627-31.

25. Janmey PA, Iida K, Yin HL, Stossel TP: Polyphosphoinositide micelles and polyphosphoinositide-containing vesicles dissociate endogenous gelsolin-actin complexes and promote actin assembly from the fast-growing end of actin filaments blocked by gelsolin. J Biol Chem 1987; 262(25): 12228-36.

26. Janmey PA, Stossel TP: Modulation of gelsolin function by phosphatidylinositol 4,5-bisphosphate. Nature 1987; 325(6102): 362-4.

27. Mullins RD, Heuser JA, Pollard TD: The interaction of Arp2/3 complex with actin: nucleation, high affinity pointed end capping, and formation of branching networks of filaments. Proc Natl Acad Sci U S A 1998; 95(11): 6181-6.

28. Fowler VM: Tropomodulin: a cytoskeletal protein that binds to the end of erythrocyte tropomyosin and inhibits tropomyosin binding to actin. J Cell Biol 1990; 111(2): 471-81.

29. Pantaloni D, Boujemaa R, Didry D, Gounon P, Carlier MF: The Arp2/3 complex branches filament barbed ends: functional antagonism with capping proteins. Nat Cell Biol 2000; 2(7): 385-91.

30. Machesky LM, Mullins RD, Higgs HN, et al.: Scar, a WASp-related protein, activates nucleation of actin filaments by the Arp2/3 complex. Proc Natl Acad Sci U S A 1999; 96(7): 3739-44.

31. Svitkina TM, Borisy GG: Arp2/3 complex and actin depolymerizing factor/cofilin in dendritic organization and treadmilling of actin filament array in lamellipodia. J Cell Biol 1999; 145(5): 1009-26.

32. Carlier MF, Laurent V, Santolini J, et al.: Actin depolymerizing factor (ADF/cofilin) enhances the rate of filament turnover: implication in actin-based motility. J Cell Biol 1997; 136(6): 1307-22.

33. Carlier MF, Pantaloni D: Control of actin dynamics in cell motility. J Mol Biol 1997; 269(4): 459-67.

34. Kwiatkowski DJ: Functions of gelsolin: motility, signaling, apoptosis, cancer. Curr Opin Cell Biol 1999; 11(1): 103-8.

35. Janmey PA, Chaponnier C, Lind SE, Zaner KS, Stossel TP, Yin HL: Interactions of gelsolin and gelsolin-actin complexes with actin. Effects of calcium on actin nucleation, filament severing, and end blocking. Biochemistry 1985; 24(14): 3714-23.

36. Yin HL, Stossel TP: Control of cytoplasmic actin gel-sol transformation by gelsolin, a calcium-dependent regulatory protein. Nature 1979; 281(5732): 583-6.

37. Yin HL, Zaner KS, Stossel TP: Ca2+ control of actin gelation. Interaction of gelsolin with actin filaments and regulation of actin gelation. J Biol Chem 1980; 255(19): 9494-500.

38. Selden LA, Kinosian HJ, Estes JE, Gershman LC: Impact of profilin on actin-bound nucleotide exchange and actin polymerization dynamics. Biochemistry 1999; 38(9): 2769-78.

39. Goldschmidt-Clermont PJ, Machesky LM, Doberstein SK, Pollard TD: Mechanism of the interaction of human platelet profilin with actin. J Cell Biol 1991; 113(5): 1081-9.

40. Safer D, Nachmias VT: Beta thymosins as actin binding peptides [published erratum appears in Bioessays 1994 Aug;16(8):590]. Bioessays 1994; 16(7): 473-9.

41. Loisel TP, Boujemaa R, Pantaloni D, Carlier MF: Reconstitution of actin-based motility of Listeria and Shigella using pure proteins. Nature 1999; 401(6753): 613-6.

42. Luby-Phelps K, Taylor DL, Lanni F: Probing the structure of cytoplasm. J Cell Biol 1986; 102(6): 2015-22.

43. Satcher RL, Jr., Dewey CF, Jr.: Theoretical estimates of mechanical properties of the endothelial cell cytoskeleton [see comments]. Biophys J 1996; 71(1): 109-18.

44. Hartwig JH, Shevlin P: The architecture of actin filaments and the ultrastructural location of actin-binding protein in the periphery of lung macrophages. J Cell Biol 1986; 103(3): 1007-20.

45. Hartwig JH, Tyler J, Stossel TP: Actin-binding protein promotes the bipolar and perpendicular branching of actin filaments. J Cell Biol 1980; 87(3 Pt 1): 841-8.

46. Ohta Y, Suzuki N, Nakamura S, Hartwig JH, Stossel TP: The small GTPase RalA targets filamin to induce filopodia. Proc Natl Acad Sci U S A 1999; 96(5): 2122-8.

47. Cunningham CC, Gorlin JB, Kwiatkowski DJ, et al.: Actin-binding protein requirement for cortical stability and efficient locomotion. Science 1992; 255(5042): 325-7.

48. Nunnally MH, Powell LD, Craig SW: Reconstitution and regulation of actin gel-sol transformation with purified filamin and villin. J Biol Chem 1981; 256(5): 2083-6.

49. Sund SE, Axelrod D: Actin dynamics at the living cell submembrane imaged by total internal reflection fluorescence photobleaching. Biophys J 2000; 79(3): 1655-69.

50. Fisher GW, Conrad PA, DeBiasio RL, Taylor DL: Centripetal transport of cytoplasm, actin, and the cell surface in lamellipodia of fibroblasts. Cell Motil Cytoskeleton 1988; 11(4): 235-47.

51. Tardy Y, McGrath JL, Hartwig JH, Dewey CF: Interpreting photoactivated fluorescence microscopy measurements of steady-state actin dynamics. Biophys J 1995; 69(5): 1674-82.

52. Witke W, Sharpe AH, Hartwig JH, Azuma T, Stossel TP, Kwiatkowski DJ: Hemostatic, inflammatory, and fibroblast responses are blunted in mice lacking gelsolin. Cell 1995; 81(1): 41-51.

53. Janmey PA, Chaponnier C: Medical aspects of the actin cytoskeleton. Curr Opin Cell Biol 1995; 7(1): 111-7.

54. Hartwig JH: Mechanisms of actin rearrangements mediating platelet activation. J Cell Biol 1992; 118(6): 1421-42.

55. Davies PF: Flow-mediated endothelial mechanotransduction. Physiol Rev 1995; 75(3): 519-60.

Chapter II

Modeling Actin Filament Dynamics in Purified Solutions

Actin filaments fill the cell cytoplasm in vivo and form a dynamic network that is actively remodeled when a cell moves. Various actin-associated proteins (reviewed in Chapter I) drive actin dynamics inside cells. In cells, actin filaments are predominately crosslinked by proteins that bind adjacent filaments [1], thereby fixing them in space and hindering their mobility. Therefore, filament dynamics in cells are primarily a result of turnover of actin polymer. In purified solutions of actin, however, no such crosslink-mediated restrictions on filament motion occur, and thus filaments may diffuse through the entangled F-actin network in addition to cycling their subunits.

In purified solutions of actin at physiological salt and ATP levels, actin spontaneously polymerizes into filaments of various lengths. At long times after initiation of polymerization, a steady state is reached in which there is no net actin polymerization and the actin filament length distribution is stable. In the absence of convection, purified actin gels exhibit three dynamic processes. First, unpolymerized monomer may diffuse throughout the buffer. Second, filaments may cycle in an ATP-dependent process, predominately adding actin monomer onto the barbed end and losing monomer from the pointed end. In this way, actin subunits flux through filaments and exhibit treadmilling behavior. Finally, without crosslinking proteins, actin filaments may diffuse. If these processes can be distinguished from one another in reconstituted, purified actin networks, then analysis of the mechanisms controlling actin dynamics is possible.

This chapter develops theory to isolate the three dynamic processes of purified actin in photoactivation of fluorescence (PAF) experiments. This is accomplished by examining the theoretical time scale of each of these events and their dependence on physical parameters, such as the properties of actin and the width of the photoactivated band. Using this knowledge, experiments are developed in Chapter III to extract information

about actin dynamics in purified solutions and compare how these processes are altered by the addition of actin regulatory proteins.

METHODS

Photoactivation of fluorescence

Photoactivation of fluorescence (PAF) involves liberating the fluorescence of a non-fluorescent precursor molecule in a small region and measuring the fluorescence decay in this region over time. For measurement of purified actin dynamics, actin monomers are fluorescently labeled and 'caged' by coupling an ultraviolet (UV) light sensitive moiety to the photosensitive group on the fluorophore, causing the normally fluorescent species to become non-fluorescent [2, 3]. PAF experiments are initiated by exposing caged actin to UV light in a specified geometry (typically circular or rectangular). Once the actin is uncaged, the fluorescence at the center of the photoactivated region is monitored over time. Using an interpretive model that describes the physics of the actin transport processes underlying the fluorescence decay, appropriate physical parameters can be extracted and analyzed [4].

The Tardy Model

A model describing PAF-based actin dynamics in cells, the Tardy Model [4], allows calculation of the fraction of total actin incorporated into actin filaments (*PF*), the diffusion coefficient of actin monomer (D_m), and the average time for actin filament turnover (τ). These three parameters are computed from the fluorescence decay in a rectangular, photoactivated band. Although this model was developed to analyze cellular actin dynamics, the simplified geometry and assumptions inherent in the theory are even better suited for analyzing purified actin dynamics.

The Tardy Model employs certain simplifying assumptions to create a tractable mathematical formulation of the problem.

1. The cell is modeled as a rectangle of constant thickness (Fig. 2-1). Photoactivation across the entire width and thickness of the model cell results in one-dimensional actin dynamics in the x-direction. The nucleus and cellular organelles are not included in the model. Since purified solutions of actin in glass tubes are this shape and lack organelles to disrupt the actin structure, this simplification is extremely accurate.

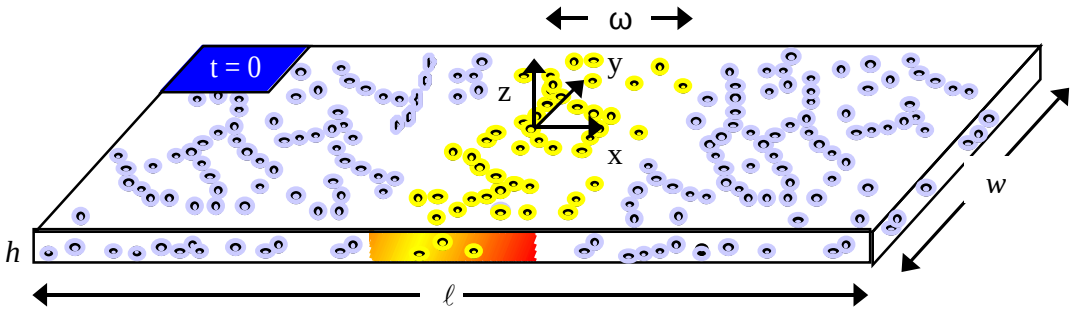

Fig. 2-1. *Simplified cell for analysis of PAF experiments.* The geometry of the cell is as shown, where $h << \ell, w$. The shaded region in the center of the model cell represents an uncaged, fluorescent actin band of width, ω, immediately after photoactivation. (adapted from Ref. [4])

2. Actin is distributed homogeneously across the model cell, disregarding actin concentrates or bundles that exist in cells, particularly in the cell cortex. Again, this assumption is valid in purified actin solutions because actin is uniformly distributed and does not contain actin bundling proteins.

3. Two interacting pools of actin, monomeric and filamentous, are dynamically coupled to each other. Actin filaments cycle subunits on and off their ends in direct exchange with the monomer pool. Actin monomer is free to diffuse, but filaments are assumed to be non-diffusible. In cells, the idealization of immobile filaments is valid since cortical actin networks are highly crosslinked by filamin

[1] and filaments diffuse much slower than the rates of cellular actin filament turnover. In purified solutions, the restriction on actin filament diffusion must be relaxed since filament turnover and diffusion may occur on similar time scales. For example, if nearly all of the actin is polymerized and the rate of filament turnover is much slower than filament diffusion, then the actin monomer diffusion coefficient calculated with the Tardy Model corresponds to the actin filament diffusion coefficient.

4. Actin dynamics are at steady state. This simplification requires that there is no net growth or diminishment of the actin monomer and filamentous pools, change in the length distributions of filaments, and generation or degradation of actin. This condition must hold on the global level within cells, since cellular movements occur on time scales much shorter than protein degradation and synthesis. However, local heterogeneities and actin transients within cells challenge this idealization. In purified, reconstituted actin networks at long times, actin dynamics are inherently at steady state as described by the kinetics of actin polymerization (Fig. 1-2).

5. The rate of actin exchange between monomer and filaments is assumed uniform throughout the model cell. This is a simplifying assumption for actual cells, but in a purified solution of proteins, a uniform rate of actin turnover should be extremely valid.

The general mathematical problem defined in the Tardy Model involves a set of unsteady, coupled partial differential equations that describe actin monomer and filament transport in the model cell. These equations are derived from first principles given the previously mentioned simplifying assumptions.

$$\frac{\partial c_{um}}{\partial t} = D_m \frac{\partial^2 c_{um}}{\partial x^2} + \dot{g}\left(\frac{c_{uf}}{c_f} - \frac{c_{um}}{c_m}\right) \tag{2.1}$$

$$\frac{\partial c_{uf}}{\partial t} = \dot{g}\left(c_{uf} - \frac{c_{um}}{c_m} c_f\right) \tag{2.2}$$

In these equations, c_{um} and c_{uf} describe the uncaged actin monomer and filament concentrations, respectively, whereas c_m and c_f describe the total actin monomer and filament concentrations, respectively. D_m is the actin monomer diffusion coefficient. The uniform rate of monomer exchange between the monomeric and filamentous pools is denoted $\dot{g}$. These equations are subject to boundary conditions stipulating that the spatial rate of change of uncaged monomer is zero at the model cell boundaries,

$$\left.\frac{\partial c_{um}}{\partial x}\right|_{x=0,\ell} = 0 \tag{2.3}$$

and initial conditions where monomer residing outside of the photoactivated band is nonfluorescent, while that contained within the band is fluorescent.

$$\left.\begin{aligned} c_{um} = c_{uf} &= 0 \\ c_{um} &= \alpha c_m \\ c_{uf} &= \alpha c_f \end{aligned}\right\} \quad |x - x_0| > \tfrac{1}{2}\omega \tag{2.4}$$

In these equations, α represents the fraction of total actin in the photoactivated band that is uncaged. In purified protein experiments $\alpha \sim 0.6$, given that ~ 60% of the actin in the band is labeled, and assuming 100% of that actin is uncaged.

Solution of the general Tardy Model. The general solution to the Tardy Model is found via a Fourier-LaPlace transform, and is represented as an infinite series for both actin monomer and filament concentrations [4]. The fluorescence intensities, *F(t)*, measured in PAF experiments are proportional to a weighted sum of the actin monomer and polymer concentrations, the excitation light intensity (I_o), and the quantum efficiency (Q) of the fluorophore.

$$F = I_o Q(c_{uf} + c_{um}) \tag{2.5}$$

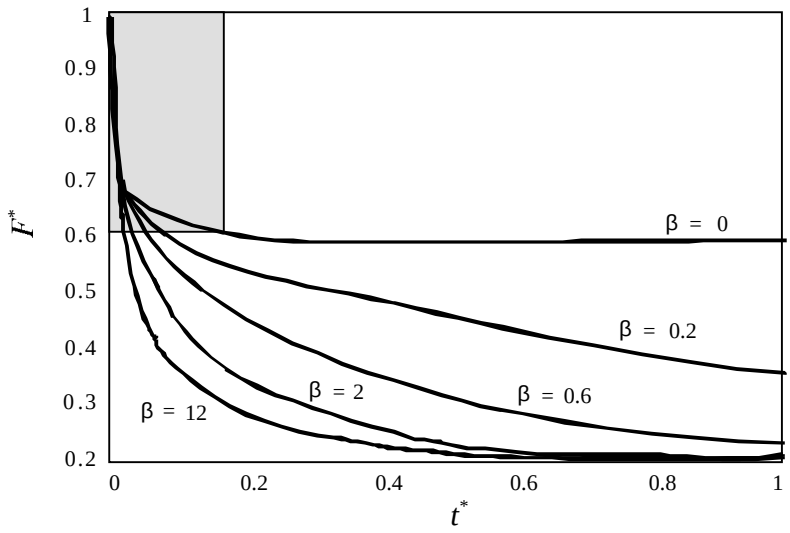

Fig. 2-2. β *dependence of fluorescence decay*. Simulations with the Tardy Model (γ = 1; $\frac{\omega}{\ell}$ = 0.2) predict a biphasic fluorescence decay; the shaded area corresponds to the actin monomer diffsuion regime, and the decay at long times is dependent on the rate of actin filament turnover. (from Ref. [4])

Nondimensionalizing the equations of the Tardy Model results in a useful parameter, β, which is the ratio of the time required for actin monomer to diffuse from the photoactivated band to the actin filament turnover time.

The general solution at long times depends strongly on β (Fig. 2-2). The fluorescence decay is biphasic, in which the rapid decay is primarily due to actin monomer diffusion, and the slow decay primarily due to actin filament turnover. The rates of decay, and the distribution of fluorescence between the two phases determines *PF*, τ, and D_m.

Simplification of the general Tardy Model solution. If actin monomer diffusion is fast enough compared to actin filament turnover, expressed as the criterion β < 4, then the solution to the general Tardy Model may be simplified to analyze fluorescence decay once actin monomer diffusion is complete ($t > 4\tau_{Dm}$) [4]. This equation is simplified further if $\omega << \ell$.

$$F = \frac{F}{F_o} = \left(\frac{c_f}{c_m + c_f}\right) e^{-\frac{t}{4\tau}} \qquad (2.7)$$

When actin dynamics are not diffusion limited, the fluorescence evolution in a photoactivated band at long times decays as a simple exponential with time constant, τ,

and y-intercept *PF*. For a typical PAF experiment, $\ell \sim 60$ μm, $D_m \sim 3$ μm^2/s, and $\tau > 10$ min; therefore $\beta < 4$ and the simplified model applies. The values for most *in vitro* and *in vivo* PAF experiments correspond to $\beta < 4$.

Dynamics at short times

At short times, monomer diffusion from the photoactivated band dominates actin dynamics. This is due to the relatively small size and shape of an actin monomer with respect to that of polymeric actin filaments, a parameter quantitated by the diffusion coefficient of each species. The time scale at which monomer diffuses can be approximated using physical arguments.

Actin monomer diffusion. Monomer diffusion from photoactivated bands is modeled as a one-dimensional, unsteady process. At constant temperature in a stationary fluid with no chemical reactions or mass generation, the transport of monomer is described by a second order partial differential equation.

$$\frac{\partial c_{um}}{\partial t} = D_m \frac{\partial^2 c_{um}}{\partial x^2} \tag{2.8}$$

In this equation, c_{um} is the uncaged actin monomer concentration in the photoactivated band; D_m is the diffusion coefficient for actin monomer; and x is the distance along the length of the model cell measured from the centerline of the photoactivated band (Fig. 2-1).

In order to determine the time scale at which actin monomer diffuses from a photoactivated band, the following scaling is introduced. Time is scaled according to a characteristic diffusion time for actin monomer (τ_{D_m}). The initial amount of uncaged monomer in the photoactivated band (c_{um_0}) scales c_{um}. The appropriate length scale for monomer diffusion in PAF experiments is the width of the photoactivated band (ω). D_m is

a physical constant, determined experimentally, describing monomer mobility in a particular fluid. Substituting into Eq. 2.8.

$$\tau_{D_m} \sim \frac{\omega^2}{D_m} \tag{2.9}$$

Therefore, the characteristic time for actin monomer diffusion from a photoactivated band is dependant on the width of the photoactivated band and the diffusion coefficient of actin monomer.

Dynamics at long times

At long times, two dynamic processes compete in photoactivated band fluorescence decay: actin filament diffusion and actin filament turnover. The time scales describing these processes can be estimated based on knowledge of the kinetics and physics underlying actin filament dynamics.

Actin filament diffusion. Actin filaments, like many semi-flexible polymers, diffuse along their length by reptation, which is a snake-like motion of the actin filament through an entangled network driven by thermal energy [5]. Actin filament diffusion perpendicular to the long filament axis is negligible [6]. The governing transport equation for one-dimensional, unsteady actin filament diffusion in a fluid at rest under constant temperature with no actin generation or chemical reactions is analogous to that developed for monomer diffusion (Eq. 2.8).

$$\frac{\partial c_{uf}}{\partial t} = D_f \frac{\partial^2 c_{uf}}{\partial x^2} \tag{2.10}$$

The concentration of uncaged actin monomer incorporated into filaments in the photoactivated band is denoted c_{uf}, and D_f is the diffusion coefficient for actin filaments along their length.

The time scale for filament diffusion from a photoactivated band can be estimated from Eq. 2.10. Time is scaled by a characteristic filament diffusion time (τ_{D_f}), and the uncaged polymerized actin monomer concentration (c_{uf}) is scaled according to the initial amount present in the photoactivated band (c_{uf_0}). As described for scaling monomer diffusion, the appropriate length scale for filament diffusion is the width of the photoactivated band (ω). The actin filament diffusion coefficient (D_f) describes the mobility of filaments along their length, and depends strongly on the actin concentration (c_a) and average actin filament length (L_{avg}) in semi-dilute solutions (2 μM < c_a < 50 μM) [6]. Assuming the diffusion of semi-flexible actin filaments is similar to stiff rods allows determination of D_f for any actin filament length but overestimates experimental filament mobility within a factor of ~20 [6].

$$D_f = \frac{k_B T \ln\left(\frac{L_{avg}}{b}\right)}{2\pi\eta L_{avg}} \tag{2.11}$$

The viscosity of water at T = 20°C (293 K) is $\eta = 1\times10^{-9}$ kg/(μm·s), and Boltzman's Constant is $k_B = 1.38\times10^{-23}$ J/K. The diameter of an actin filament is $b \approx 7$ nm. Scaling Eq. 2.10 according to τ_{D_f}, D_f, and ω allows computation of the characteristic time scale for actin filament diffusion from a photoactivated band.

$$\tau_{D_f} \sim \frac{\omega^2}{D_f} \tag{2.12}$$

Therefore, the actin filament diffusion time depends on D_f, a function of the average actin filament length and the width of the photoactivated band.

Actin filament turnover. At steady state, actin filaments cycle their individual monomeric subunits at known rates. On average, assuming a treadmilling model of actin filament turnover, actin monomers charged with ATP predominately assemble at the barbed end because of the ~10-fold greater affinity of ATP-actin at this end of the filament [7]. After

assembly, ATP-actin is hydrolyzed to ADP•Pi-actin, followed by slow dissociation of Pi from actin filament subunits as they flux towards the pointed end. At the actin filament pointed end, ADP F-actin subunits dissociate, and are subsequently recharged with ATP in the actin monomer pool. While the true nature of actin dynamics is more complex, the treadmilling approximation for actin filament turnover is considered valid for low concentrations of actin, near the critical concentration of ATP-actin for the pointed end (C_{c_p} = 0.6 μM) [7-9]. Under these conditions, filament elongation is only observed at the barbed end of actin filaments [10].

The time rate of change of actin filament length at the barbed and pointed ends can be described by first order differential equations accounting for the kinetics of actin monomer association and dissociation.

$$\begin{aligned} \frac{dL_b}{dt} &= K_{bT}^{+} c_m \\ \frac{dL_p}{dt} &= -K_{pD}^{-} \end{aligned} \tag{2.13}$$

L_b and L_p are the actin filament lengths at the barbed and pointed ends, respectively; c_m is the actin monomer concentration; K_{bT}^{+} is the ATP-actin monomer association rate constant at the barbed end; and K_{pD}^{-} is the rate constant for ADP-actin subunit dissociation at the pointed end. At steady state, because there is no net actin polymerization, the rate of actin filament elongation at the barbed end equals filament disassembly at the pointed end.

$$\frac{dL_b}{dt} = \frac{dL_p}{dt} \tag{2.14}$$

For simplicity, the characteristic time scale for actin filament turnover (τ_t) at steady state will be formulated according to the rate of subunit loss at the pointed end of the actin filament, rather than the kinetics at the barbed end, since these are equivalent. The average length of actin filaments (L_{avg}) scales L_p, and the kinetic rate constant K_{pD}^{-} is

determined experimentally. Given the above arguments for a treadmilling model at steady state, the characteristic actin filament turnover time is proportional to the rate of ADP-actin subunit dissociation at the pointed end and the average length of actin filaments.

$$\tau_t \sim \frac{L_{avg}}{K_{pD}^-} \tag{2.15}$$

Values for the ADP-actin pointed end dissociation rate constant are taken from the published values as $K_{pD}^- = 0.03 - 0.4\ s^{-1}$, depending on the reference source [7, 8, 11, 12].

Computation and simulations

The computational software package Matlab 5.2 (v. 1.62, The Mathworks, Natick, MA) was used to model the time scales of actin dynamics and perform Tardy Model simulations. The Tardy Model was coded in C++, compiled, and run remotely via a Matlab script. Computer algorithms were executed on a Macintosh G3 computer (Apple, Cupertino, CA).

RESULTS

At long times in PAF experiments, actin filament diffusion and filament turnover determine the fluorescence decay properties of photoactivated bands. If these two processes can be isolated, the functions of purified actin-regulatory proteins on filament dynamics can be examined to either confirm previously proposed mechanisms of action or infer new, undiscovered functions. Based on the modeling, isolation of actin filament turnover and diffusion is theoretically possible simply by altering the width of the photoactivated band.

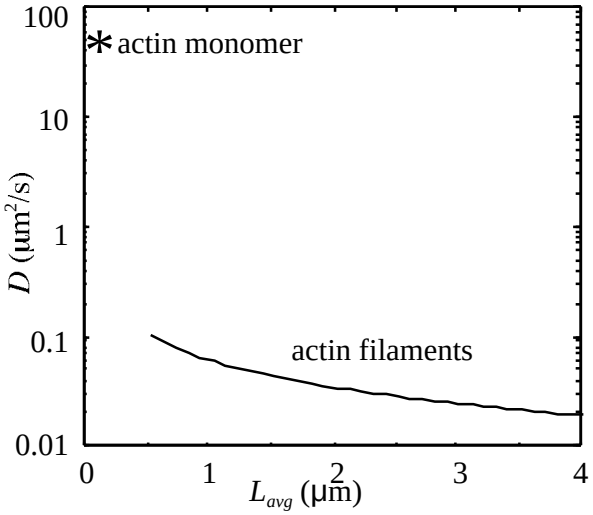

Fig. 2-3. *Diffusion coefficient of actin monomer and filaments.* Actin monomer is approximately three orders of magnitude more mobile than filaments. (data from Refs. [6, 13])

Diffusion coefficients for actin monomer and filaments

In a given solute, actin monomer has a constant diffusivity, while the mobility of actin filaments is dependent on filament length. These physical constants are determined experimentally. PAF experiments on unpolymerized, purified actin (see Chapter III) estimate the actin monomer diffusion coefficient at $D_m \approx 56\ \mu m^2/s$. This value is consistent with the consensus value for monomer mobility in aqueous solution of $D_m = 71.5\ \mu m^2/s$ [13]. Actin filament diffusion coefficients, as predicted by Eq. 2.11, are orders of magnitude less than for monomer at any filament length (Fig. 2-3).

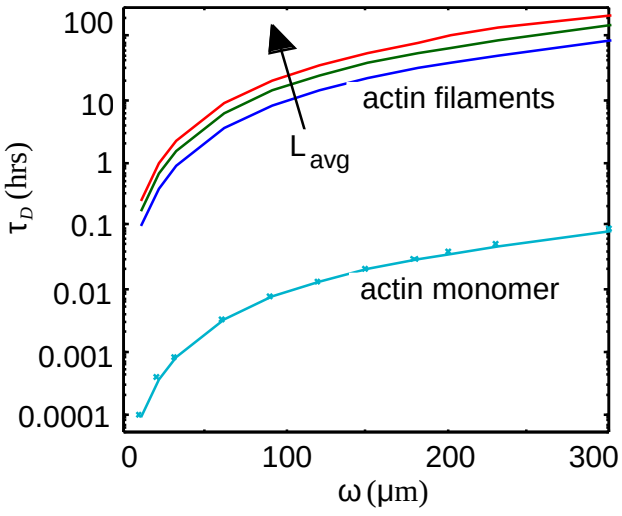

Fig. 2-4. *Theoretical purified actin diffusion time scales*. Actin monomer diffusion is on the order of seconds and is orders of magnitude faster than actin filament diffusion.

Diffusion times for actin monomer and filaments

The time scale for a one-dimensional, purely diffusive process in a photoactivated band depends explicitly on the width of the photoactivated band and the diffusion coefficient of the mobile species. Eqs. 2.9 and 2.12 describe the characteristic time

scales of these processes. According to these approximations, actin monomers diffuse from a photoactivated band on the order of seconds, while filaments require hours (Fig. 2-4). Therefore, monomer diffusion and filament diffusion can be isolated from each other ($\tau_{D_m} << \tau_{D_f}$); within minutes after photoactivation, monomer will have completely diffused from the photoactivated band and subsequent diffusion can be attributed solely to filaments.

Turnover times for actin filaments

In photoactivated bands, actin filaments turnover and lose fluorescent subunits from their ends. According to Eq. 2.15, the filament turnover time at steady state depends on the length of actin filaments and the rate of loss at the pointed end, but is independent of the width of the photoactivated band as long as the criterion $\tau_t >> \tau_{D_m}$ is satisfied. Therefore, the characteristic time for actin filaments to turnover at a given length is on the order to hours (Fig. 2-5).

Isolating actin filament turnover from actin filament diffusion

The time scales for actin filament diffusion and turnover at steady state (Eqs. 2.12 and 2.15) are both related to the length of actin filaments, but only the filament diffusion time is dependent on the width of the photoactivated band. Therefore, altering the width of the photoactivated band can preferentially select one dynamic process to occur more rapidly than the other. This implies that, in an experiment with the same average filament length, by using different sized photoactivated bands actin filament diffusion and turnover can be isolated from one another. Comparison of the time scales of actin filament diffusion and turnover allows selection of appropriate photoactivated band widths (Fig. 2-5). Choice of a wide, 230 μm photoactivated band slows actin filament diffusion tremendously, resulting in fluorescence decay due solely to actin filament turnover. Alternatively, selecting a narrow, 30 μm photoactivated band theoretically produces actin filament

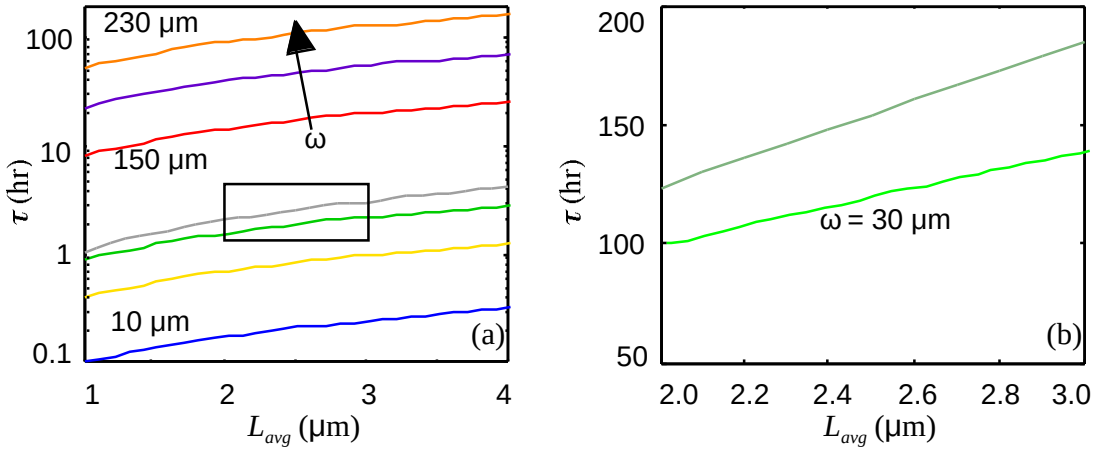

Fig 2-5. *Separating actin filament diffusion and turnover*. (a) Actin filament diffusion (solid lines) depends on the width of the photoactivated band, but turnover (dotted line) does not. ω = 230 μm results in actin filament turnover occurring much faster than filament diffusion. (b) For ω = 30 μm, scaling predicts that filament diffusion times are approximately equivalent to turnover times.

diffusion and turnover times of approximately the same order of magnitude. In this case, both actin filament diffusion and turnover are responsible for photoactivated band fluorescence decay. While photoactivated bands of < 30 μm would be ideal for isolating actin filament diffusion from turnover, this is not possible because of limits in the resolution of the PAF microscopy system and complications in the analysis of actin filament dynamics as the photoactivated band width approaches the order of magnitude of the lengths of actin filaments ($\omega \rightarrow L_{avg}$).

Narrow photoactivated bands

Simulations with the generalized Tardy Model were performed to represent narrow photoactivated band PAF experiments. From these simulations, spatial and temporal fluorescence profiles of photoactivated band decay can be generated, providing theoretical limits for narrow band PAF experiments in which actin filament diffusion and turnover times are comparable. The narrow band simulation exhibits a fluorescence profile that simultaneously broadens and decays (Fig. 2-6a). Photoactivated band broadening is the hallmark of actin filament diffusion, while fluorescence decay is a result of both dynamic processes. Nondimensionalizing the centerline photoactivated

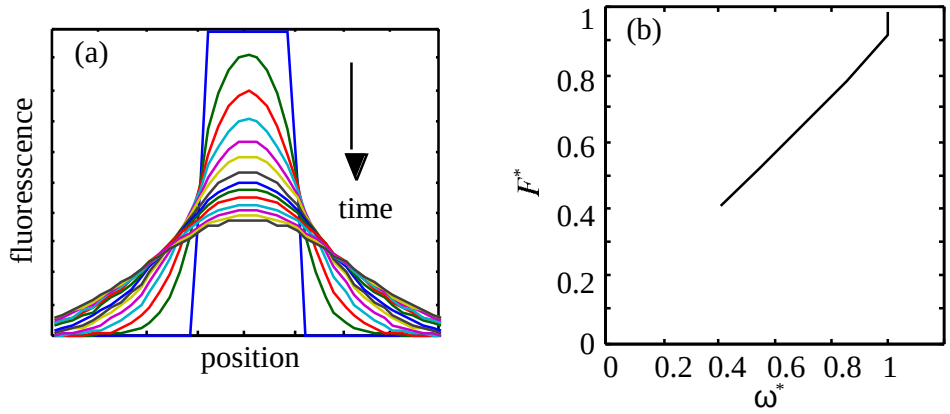

Fig. 2-6. *Narrow photoactivated band Tardy Model simulations*. (a) The spatial fluorescence profile for a narrow band simultaneously broadens and decays over time. (b) Quantitation of the fluorescence decay and band width changes reveals the theoretical bound for the actin filament diffusion and turnover regime associated with narrow photoactivated band fluorescence decay.

band fluorescence, $F(t)$, and the width of the photoactivated band, $\omega(t)$, with their initial values F_0 and ω_0, respectively, creates parameters independent of variations in initial fluorescence intensities and photoactivated band widths to facilitate comparison of simulations and experiments performed under different conditions.

$$F^* = \frac{F(t)}{F_0}$$
$$\omega^* = \frac{\omega(t)}{\omega_0} \qquad (2.16)$$

A nondimensional plot of F^* and ω^* sets the theoretical limits for the regime of simultaneous actin filament diffusion and turnover (Fig 2-6b).

Wide photoactivated bands

PAF experiments with wide photoactivated bands, in which the time for actin filament diffusion is much slower than that for filament turnover, were simulated with the generalized Tardy Model. Wide photoactivated bands theoretically decay via actin filament turnover. Simulations reveal that the wide band spatial fluorescence profiles decay without broadening, confirming the slow rate of filament diffusion from the

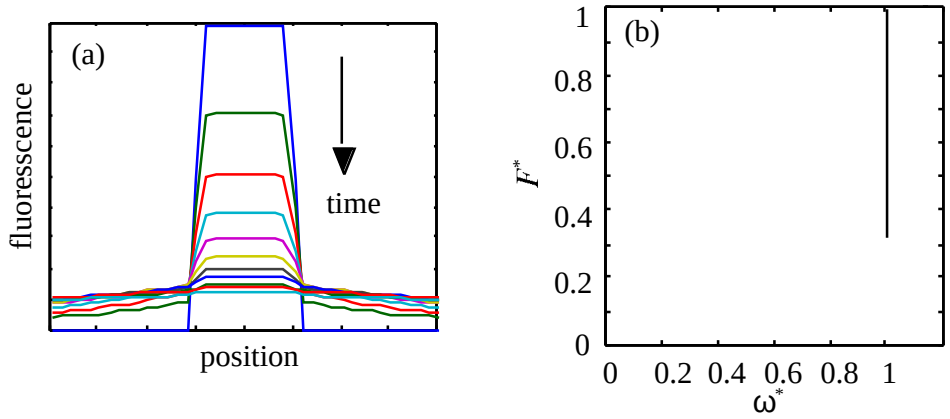

Fig. 2-7. *Wide photoactivated band Tardy Model simulations*. (a) The spatial fluorescence profile for a wide band decays without broadening. (b) Quantitation of F^* vs. ω^* reveals the theoretical bound for the actin filament turnover regime associated with wide photoactivated band fluorescence decay.

photoactivated band (Fig. 2-7a). A nondimensional plot of F^* and ω^* characterizes filament turnover in wide photoactivated bands and sets the theoretical limits for the actin filament turnover regime (Fig. 2-7b).

DISCUSSION

Photoactivation of fluorescence is an ideal method to noninvasively measure actin dynamics in purified protein solutions. The Tardy Model is well suited to infer parameters that described the dynamics of actin, such as the fraction of total actin polymerized and the lifetime of actin filaments, simultaneously on the same preparation of purified actin. Simulations and theory describing the processes that occur in photoactivated bands of purified actin clearly reveal the differences between actin diffusion and turnover.

In a stationary, homogeneous, purified actin preparation at steady state with constant temperature, no chemical reactions or mass generation, and an excess of ATP, fluorescent bands of actin decay by diffusion of actin monomer and filaments and by cycling of actin subunits through filaments. In order to isolate the dynamic processes that occur in

purified actin solutions, mathematical equations describing actin filament diffusion and turnover were scaled to reveal the characteristic times at which these processes proceed. Actin monomer and filament diffusion times scale according to the width of the photoactivated band and the mobility of each species (Eqs. 2.9 and 2.12). Since the characteristic actin monomer diffusion time is orders of magnitude slower than that of actin filament diffusion and actin filament turnover (Eq. 2.15), monomer diffusion occurs seconds to minutes after photoactivation. Alternatively, filament diffusion occurs hours after photoactivation, depending on the width of the photoactivated band and average filament length. In a process independent of the photoactivated band width, filaments continuously cycle actin subunits, which, depending on the kinetics and filament length, determines the actin filament lifetime.

Theoretically, actin filament diffusion and turnover compete at long times in photoactivated bands of actin, after monomer diffusion is complete. Actin filament diffusion scales according to the width of the photoactivated band, but the time scale of actin filament turnover is independent of the photoactivated band width. Therefore, actin filament turnover can be theoretically isolated from actin filament diffusion with a wide, 230 μm photoactivated band, which produces a characteristic spatial fluorescence profile that decays without broadening. Narrow photoactivated bands decay as a result of a combination of actin filament diffusion and turnover, evidenced by simulations that predict simultaneous photoactivated band decay and broadening. PAF experiments in purified actin solutions with narrow and wide photoactivated bands, based on this theory, are explored in depth in Chapter III.

REFERENCES

1. Hartwig JH, Shevlin P: The architecture of actin filaments and the ultrastructural location of actin-binding protein in the periphery of lung macrophages. J Cell Biol 1986; 103(3): 1007-20.

2. McCray JA, Trentham DR: Properties and uses of photoreactive caged compounds. Annu Rev Biophys Biophys Chem 1989; 18: 239-70.

3. Theriot JA, Mitchison TJ: Actin microfilament dynamics in locomoting cells. Nature 1991; 352(6331): 126-31.

4. Tardy Y, McGrath JL, Hartwig JH, Dewey CF: Interpreting photoactivated fluorescence microscopy measurements of steady-state actin dynamics. Biophys J 1995; 69(5): 1674-82.

5. Kas J, Strey H, Sackmann E: Direct imaging of reptation for semiflexible actin filaments. Nature 1994; 368(6468): 226-9.

6. Kas J, Strey H, Tang JX, et al.: F-actin, a model polymer for semiflexible chains in dilute, semidilute, and liquid crystalline solutions. Biophys J 1996; 70(2): 609-25.

7. Pollard TD: Rate constants for the reactions of ATP- and ADP-actin with the ends of actin filaments. J Cell Biol 1986; 103(6 Pt 2): 2747-54.

8. Korn ED, Carlier MF, Pantaloni D: Actin polymerization and ATP hydrolysis. Science 1987; 238(4827): 638-44.

9. Bonder EM, Fishkind DJ, Mooseker MS: Direct measurement of critical concentrations and assembly rate constants at the two ends of an actin filament. Cell 1983; 34(2): 491-501.

10. Wegner A: Head to tail polymerization of actin. J Mol Biol 1976; 108(1): 139-50.

11. Selve N, Wegner A: Rate of treadmilling of actin filaments in vitro. J Mol Biol 1986; 187(4): 627-31.

12. Janmey PA, Stossel TP: Kinetics of actin monomer exchange at the slow growing ends of actin filaments and their relation to the elongation of filaments shortened by gelsolin. J Muscle Res Cell Motil 1986; 7(5): 446-54.

13. Lanni F, Ware BR: Detection and characterization of actin monomers, oligomers, and filaments in solution by measurement of fluorescence photobleaching recovery [published erratum appears in Biophys J 1989 Jul;56(1):following 222]. Biophys J 1984; 46(1): 97-110.

Chapter III

Actin Filament Dynamics in Purified Solutions

In the presence of excess ATP at steady state, actin subunits continuously flux through filaments. In addition, irrespective of ATP, purified actin monomers and filaments diffuse throughout the buffer solution. Photoactivation of fluorescence (PAF) is a powerful tool to quantitate dynamic phenomena such as these in cells and purified actin solutions. As modeled in Chapter II, in purified actin solutions at steady state photoactivated bands of actin at long times decay according to two processes that compete to rearrange the actin network: actin filament diffusion and actin filament turnover. Actin filament diffusion and turnover can be isolated by altering the width of the photoactivated band because the time scales at which these processes occur depend on different physical parameters. The time scale for filament diffusion depends on the width of the photoactivated band and the diffusivity of actin filaments. In contrast, the filament turnover time is independent of the photoactivated band width. Narrow, 30 μm photoactivated bands decay due to simultaneous actin filament turnover and diffusion, whereas wide, 230 μm photoactivated bands decay predominately by actin filament turnover. In this chapter, narrow and wide photoactivated band PAF experiments are used to examine purified actin filament dynamics and determine the effect of actin filament crosslinking and stabilization on these dynamic processes.

The development of this reconstituted, purified protein system stems from an idea introduced by Dr. James L. McGrath. In his doctoral thesis, McGrath describes a system that can be used to study purified actin dynamics *in vitro* using the technique photoactivation of fluorescence [1]. This original idea is expanded and developed in Chapter II through mathematical scaling laws that describe purified actin filament dynamics in photoactivated bands, and by validation of the theory in this chapter with experiments on purified actin in the absence and presence of actin-regulatory proteins. This novel system measures actin filament dynamics at a true steady state, whereas other

investigators have inferred steady state values by extrapolating dynamic measurements [2]. Since photoactivation is a noninvasive technique, this system also improves over micropipette-based measurement techniques of actin filament dynamics [2-5]. Measurements of actin dynamics obtained in this system can then be compared to theoretical actin model predictions [6] and values obtained in cellular experiments [7-12].

METHODS

Preparation of caged resorufin actin

Rabbit α-skeletal muscle actin was prepared from acetone powder of rabbit back and leg muscle according to the method originally developed by Spudich and Watt [13]. Actin isolated in this fashion requires further purification to remove contamination by the high-affinity barbed end capping protein CapZ (M_w = 65,000), originally discovered due to reductions in the low shear viscosity of purified actin filament solutions [14, 15]. To purify actin from CapZ, the protein solution was fractionated with fast protein liquid chromatography (FPLC) on a Superose 6 sizing column (Amersham Pharmacia Biotech, Uppsala, Sweden) in Buffer A (2 mM TRIS-HCl, 0.2 mM $CaCl_2$, 0.5 mM β-mercaptoethanol, 0.5 mM ATP, pH 7.4), which separates proteins from 5 to 500 kDa based on molecular weight. Fractions collected from the column were measured for CapZ contamination by immunoblotting using a polyclonal antibody recognizing both α and β subunits of CapZ. This procedure, along with the use of low actin concentrations (< 6 μM) in PAF experiments, reduces the concentration of CapZ well below the dissociation constant (K_D ~ 1 nM) [16] of CapZ for actin, further eliminating any potential capping activity [15]. Only actin fractions determined to be free of CapZ by immunoblot were labeled with caged resorufin (CR).

CR was prepared according to the method of Theriot and Mitchison [8]. Briefly, 1-(2-nitrophenyl)diazoethane was created from a stock solution of the hydrazone of 2-

nitroacetophenone according to the method of Walker and colleagues [17]. The diazoethane was evaporated, dissolved in dimethyl formamide, and added in a 2:1 molar excess with N-(resorufin-4-carbonyl)-N'-(iodoacetyl)piperazine (Sigma, St. Louis, MO), allowing the mixture to react overnight in the dark at room temperature with continuous mixing. Following the reaction, CR was purified by separation on a preparative thin layer chromatography plate (model PLK5F; Whatman, Maidstone, Kent, UK), recovered, and eluted into 100% acetone. The acetone was evaporated and the CR dissolved in a small volume of DMSO. The spectral properties of CR, caged and uncaged, were compared to previously published fluorescence profiles and the concentration determined by measuring the absorbance of CR at 450 nm (ε_{450} = 25 $mM^{-1}cm^{-1}$) [8]. CR was stored at 4°C for later conjugation to purified actin.

Coupling of CR to ultra-purified rabbit α-skeletal muscle actin (CR-actin) was accomplished by polymerizing actin in coupling buffer (10 mM HEPES, 2 mM $MgCl_2$, 100 mM KCl, 0.5 mM ATP, pH 7.8) at 37°C. Following polymerization, a 2:1 molar excess of CR was added to the actin solution and the mixture allowed to react in the dark overnight at 4°C with constant, gentle mixing. Following the coupling of CR and actin, the solution was centrifuged at 225,000 × g for 30 min at 4°C to pellet F-actin. The pellet was dissolved in Buffer A and then dialyzed overnight into Buffer A with Slide-A-Lyzer® dialysis cassettes (Pierce Chemical Co., Rockford, IL). The labeling efficiency and concentration were determined in completely uncaged CR-actin by measuring the absorbance of resorufin and actin at 575 nm (ε_{575} = 65 $mM^{-1}cm^{-1}$) and 290 nm (ε_{290} = 26.5 $mM^{-1}cm^{-1}$), respectively. The concentration of CR-actin was confirmed by sodium dodecyl sulfate-polyacrylamide gel electrophoresis (SDS-PAGE) and digital densitometry of commassie brilliant blue (CBB) stained 10% gels. Iodacetamide derivatives, such as CR, react with sulfhydryl groups on proteins [18] such as the cysteine 374 residue (cys-374) on the actin monomer. Actin labeled at cys-374 has been shown to readily polymerize at normal pH, temperature, and salt conditions, with a critical concentration similar to unlabeled actin [19, 20]. The minimal disturbance to actin

polymerization by fluorescent labeling at this site is a result of the accessibility and position of cys-374 on the actin monomer, which is located on the periphery of actin filament subunits [21].

The competency of CR-actin polymerization was determined with a fluorescence-based actin assembly assay. Monomeric CR-actin was added in equimolar amounts to 1 μM pyrene-labeled G-actin (pyrene-actin) in a borosilicate glass test tube (Kimble/Kontes, Vineland, NJ) in the presence of Buffer B (10 mM TRIS-HCl, 0.2 mM $MgCl_2$, 100 mM KCl, 0.1 mM EGTA, 0.5 mM β-mercaptoethanol, 0.5 mM ATP, pH 7.4), briefly vortexed, and the change in pyrene fluorescence (Ex. 366 nm; Em. 388 nm) as pyrene-actin polymerizes was monitored with a luminescence spectrometer (model LS-50B; PerkinElmer Analytical Instruments, Norwalk, CT). To measure the rate of CR-actin filament elongation, short CR-actin filaments were used as preformed nucleation sites for pyrene-actin assembly. 10 μM CR-actin was polymerized in Buffer B for 2 hours at 37°C, sonicated for 10 seconds, diluted to 1 μM, and then immediately added to 1 μM pyrene-actin. The mixture was briefly vortexed and the fluorescence measured over time. The rate of actin filament elongation was calculated from the initial slope of the fluorescence curve and the initial and final fluorescence values. Pyrene-actin had a labeling efficiency of ~0.4, determined by comparing the absorbance of pyrene-actin at 344 nm (ε_{344} = 22 $mM^{-1}cm^{-1}$) [22] to unlabeled actin at 290 nm (ε_{290} = 22 $mM^{-1}cm^{-1}$).

Optimization of BSA glass coating to limit actin binding

In order to minimize actin binding to the surface of glass microcapillary tubes in PAF experiments, control experiments were performed to determine optimal concentrations of BSA to coat the tube surface and provide a substrate with a low-affinity for actin. Glass slides were coated with concentrations of 0, 0.1, 1, and 10 mg/ml BSA at 37°C, covered with 2 μM rabbit α-skeletal muscle G- or F-actin, and allowed to equilibrate for 2 hours. The glass slides were washed 3x with phosphate buffered saline (PBS) to remove

nonadherent actin molecules. Protein remaining bound to the BSA coated glass was collected by solubilization in SDS-sample buffer (62.5 mM TRIS-HCl (pH 6.8), 0.715 M β-mercaptoethanol, 10% glycerol, 2% SDS, 0.02% bromophenol blue). The concentration of F- and G-actin bound to the glass slides following coating was measured by separating protein on 10% gels by SDS-PAGE, CBB staining, digitization, and quantitation with the public domain software package NIH Image (v. 1.62; developed at the U.S. National Institutes of Health and available on the Internet at http://rsb.info.nih.gov/nih-image/) on a Macintosh G3 computer.

Photoactivation of Fluorescence

In order to load glass microcapillary tubes with ultra-purified actin, a device was created consisting of a 1 ml syringe fitted with a two-way stopcock and silicone tubing connected to a 100 µl round glass micropipette tube. Rectangular, borosilicate glass microcapillary tubes (Friedrich and Dimmock, Millville, NJ) of dimensions 0.05 × 0.5 x 50 mm were sealed onto the end of the micropipette with melted wax. Using the syringe to induce negative pressure, the microcapillary tubes were loaded with a 1 mg/ml BSA (fatty-acid poor) coating solution for 2 min at 37°C in order to minimize actin binding to the glass surface (see results). CR-actin was diluted to 2 µM from a stock solution into either Buffer A for G-actin experiments, or Buffer B to induce actin polymerization. Following dilution, CR-actin was loaded into BSA coated microcapillary tubes, the tube released from the micropipette by melting the wax seal with a gentle flame, and the ends of the microcapillary tube sealed with seal-ease® clay (Beckton Dickinson, Franklin Lakes, NJ). Microcapillary tubes filled with CR-actin were allowed to reach steady state overnight at room temperature in the dark to minimize inadvertent photoactivation.

The PAF microscopy system utilized to measure actin dynamics has been described in detail previously [23]. In brief, microcapillary tubes filled with CR-actin are placed on the stage of a modified epi-fluorescent Zeiss IM microscope (Carl Zeiss, Oberkochen,

Germany) fitted with a 16x multi-immersion Zeiss Plan-Neofluar objective (NA = 0.5). The microscope is equipped with two perpendicular mercury arc lamps that form external fluorescent light paths for photoactivation (365 nm) and global excitation (577 nm) of CR-actin. An adjustable rectangular slit in the photoactivation light path allows discrete control of the width of the photoactivation band at the sample. CR-actin fluorescence is detected with a Hamamatsu C400-50 CCD camera (Hamamatsu Corp., Hamamatsu City, Japan) equipped with an extended blue GEN III Video Intensifier (model VS4-1845; Video Scope Intl., Sterling, VA). A Macintosh G3 computer receives the digital images from the detection system via an internal Scion LG-3 framegrabber (Scion Corp., Frederick, MD) and controls the photoactivation and excitation shutter timing using automated macros written for NIH Image.

PAF experiments were initiated by irradiating the sample with a 30 or 230 μm band of photoactivating UV light, which uncages CR-actin fluorescence locally. In order to achieve bright photoactivated bands relative to the background intensity, photoactivation times were typically 5 to 10 seconds. Following photoactivation, the sample is exposed to continuous excitation for < 5 seconds to eliminate the fluorescent rise observed for CR-actin *in vitro*. This step completes the conversion of CR-actin into its fluorescent form by bypassing the aci-nitro intermediate proposed to induce a fluorescent rise in CR-actin samples outside of the highly reducing environment that exists inside cells [1]. Once completely uncaged, the time evolution of CR-actin fluorescence decay was monitored at the photoactivated band centerline and spatially across its width. CR-actin fluorescence was sampled over time with 70 ms fluorescence excitation pulses per data point in order to limit potential photobleaching artifacts. Experiments were conducted for a total of 2 hours on narrow photoactivated bands and 6 hours on wide photoactivated bands. Over each experiment, twenty independent fluorescence measurements were recorded at equally spaced time intervals. Finally, the Tardy Model was utilized to interpret the measured fluorescence profiles and compute the fraction of total actin incorporated into

actin filaments (*PF*), the actin filament turnover time (τ), and the mobility of actin monomer (D_m).

PAF experiments with purified proteins

To stabilize actin filaments against disassembly, CR-actin was polymerized in the presence of a 1:1 molar equivalent of phallacidin. Phallacidin binds to actin filaments in an equimolar complex with F-actin subunits, and inhibits depolymerization at both the barbed and pointed ends [24, 25].

To form crosslinked actin gels, CR-actin was polymerized with the *Dictyostelium discoidium* actin filament crosslinking protein ABP-120 at a molar ratio of 1:20. The required concentration of ABP-120 was determined by a falling ball assay to measure the rapid increase in the low-shear viscosity of actin filaments upon formation of a crosslinked gel as previously described [26]. ABP-120 was added to solutions of CR-actin immediately prior to microcapillary tube loading in order to eliminate shear-induced fracture and artificial alignment of the purified actin gel.

Analysis of PAF experiments

Centerline fluorescence measurements from PAF experiments were analyzed with the Tardy Model (see Chapter II), which provides a mathematical description of actin transport. This model assumes a simplified rectangular geometry and lack of cellular organelles, nucleus, actin gradients, and actin filament bundles, all of which are valid for purified actin solutions. At long times, after actin monomer has diffused from the photoactivated band, the general Tardy Model may be simplified to an Eq. 2.7 if the following two conditions are met [27].

$$\omega << \ell \text{ and } \beta < 4 \qquad (3.1)$$

The photoactivated band width, ω, and the length of the microcapillary tube, ℓ, are defined in the Tardy Model with respect to the geometry of the model cell (Fig. 2-1). In purified actin experiments, ℓ = 50 mm and ω = 30 or 230 μm. Therefore, $\omega << \ell$ is satisfied. β is a nondimensional parameter that is the ratio of the actin monomer diffusion to filament turnover times (Eq. 2.6). Theoretically, an upper bound for β in purified actin experiments is estimated to be $\beta \sim 0.2$, given D_m = 71.5 μm^2/s [28], $\tau \sim 1$ hr (computed from [2] for a 3 μm actin filament), and ω = 230 μm. Therefore, the condition $\beta < 4$ is also satisfied.

Since the criteria of Eq. 3.1 are both achieved in purified actin PAF experiments, the fluorescence decay at long times can be described adequately by Eq. 2.7, a decaying exponential where the y-intercept is the fraction of total actin incorporated into filaments (*PF*), and the decay time constant corresponds to the actin filament turnover time (τ) [27]. For narrow photoactivated bands, τ represents the characteristic time for a complex process involving both actin filament diffusion and turnover, but in wide photoactivated bands the decay constant is simply interpretated as $\tau = \tau_t$, the actin filament turnover time. Given the above arguments, all experiments for narrow and wide photoactivated bands were analyzed with the simplified Tardy Model by computing a best-fit exponential function to the fluorescence decay with Matlab (version 5.2.1; The Mathworks, Natick, MA) that minimizes the error between the fit and data in a least-squares sense.

To quantitate diffusion-mediated changes (band broadening) in PAF experiments, spatial fluorescence profiles across the band width were measured over time. High frequency noise is reduced in the profiles by averaging adjacent pixel intensities and applying a fifth-order Butterworth filter. The width of the photoactivated band was measured as the distance between spatial fluorescence profile intensity values at 50% of the maximum, also known as the full width half max (FWHM) value.

Calculation of the actin filament pointed end subunit dissociation rate

Wide photoactivated bands decay exclusively due to the turnover of actin filaments, since actin filament diffusion is relatively slow. Therefore, measuring the actin filament turnover time (τ_t) with the Tardy Model and rearranging the terms in the scaling law (Eq. 2.15) for actin filament turnover developed in Chapter II allows calculation of the ADP-actin pointed end dissociation rate constant, K_{pD}^{-}.

Deleterious effects of photoactivation on actin

Phototoxicity, photodissolution, and local heating of actin during uncaging and fluorescence excitation are important factors to consider when performing PAF experiments. These destructive processes can potentially induce actin filament and monomer crosslinking, denature actin protein structure, and break actin filaments.

Estimation of the photoactivation (~100 kW/m^2) and excitation (~10 kW/m^2) fluorescence intensities at the sample [29] classifies these light levels as low excitation intensities (< 5 MW/m^2) according to Vigers and colleagues [30]. At low light excitation levels, both actin and microtubules have the potential to fracture and dissolve (photodissolution) after as short as ~1 min of continuous illumination [30, 31]. To control for potential photodissolution, CR-actin was never exposed to more than 20 seconds of continuous fluorescence illumination, and no more than 22 seconds of total exposure over the entire course of the experiment.

Surface heating of the actin solution is less problematic during photoactivation and excitation, since even at the high laser intensities (> 5 MW/m^2) used to photobleach samples in fluorescence recovery after photobleaching (FRAP) experiments, the amount of sample heating is estimated to be less than 0.1°C [32].

F-actin phototoxicity after fluorescence exposure is further refuted by the observation that actin filaments turnover in wide photoactivated bands (see results) with lifetimes

similar to previously published values using alternative methods [3]. Macroscopic photochemical crosslinking of actin monomer or filaments is not observed, as the fluorescent band intensity is uniform with no apparent fluorescent actin bundles. Massive filament photodissolution and fracture will change the diffusive properties of actin filaments, resulting in wide photoactivated band broadening in contrast to the theory presented in Chapter II. Experiments with wide photoactivated bands exhibit no apparent broadening of the photoactivated band. Therefore, no obvious photoactivation or excitation-induced artifacts on actin filament dynamics are evident, underscoring the benign nature of photoactivation experiments.

ATP levels required for actin filament turnover

In order for actin filaments to remain dynamic, excess ATP must be present in solution to counteract ATP hydrolysis and degradation as actin filaments turnover. Due to the long time scales of actin filament diffusion and turnover, PAF experiments in purified solutions of actin are performed over the span of several days. There must be sufficient amounts of ATP available to support continual recharging of the ATP-actin monomer pool.

Assuming a treadmilling model of actin filament turnover at steady state, the time after actin polymerization in which turnover is not ATP-limited depends on the rate of actin filament subunit flux ($\vec{q}$), and the total number of actin filaments available for polymerization (n_f). Selve and Wegner measured the rate of actin flux *in vitro* at $\vec{q}$ = 2 μm/hr [3]. This is related to the filament turnover time (τ) according to $\tau = \frac{L_{avg}}{\vec{q}}$, and therefore, assuming L_{avg} = 3 μm, then τ = 1.5 hr. The rate at which ATP is hydrolyzed on actin filament subunits has been published at $K_{T\text{-}D\text{•}Pi} = 0.023\ s^{-1}$, and is independent of the actin concentration [33]. Since the time required for ATP hydrolysis on actin filaments, $t_{T\text{-}D\text{•}Pi} = \frac{1}{K_{T-D\text{•}Pi}} \sim 1$ min, is much shorter than the actin filament turnover time, the rate of actin filament subunit flux limits the rate of ATP consumption and every ATP-actin

monomer that assembles into an actin filament has sufficient time to be hydrolyzed. Under these conditions, the rate of actin filament subunit flux is equivalent to the rate of ATP consumption per actin filament. Given a total actin concentration of 2 μM and the ATP-actin critical concentration at $C_{c\text{-}ATP} \approx$ 0.1 μM [34], the total number of actin filaments per microcapillary tube is estimated as $n_f = 1.3\times10^9$, equivalent to the number of uncapped barbed and pointed actin filament ends. Using the estimates for n_f and $\vec{q}$, ATP is consumed at a rate of 9.6×10^{11} hr^{-1}. Therefore, since 0.5 mM ATP is present in actin polymerization buffer (Buffer B) and taking into account ATP degradation in solution, conservatively, ATP will remain at sufficient levels to drive actin filament turnover for at least three days following actin polymerization.

Measurement of actin filament lengths

The average actin filament length (L_{avg}) for each PAF experiment was determined by negative staining and electron microscopy. To prevent sample evaporation, a hydrated chamber was prepared by placing filter paper, saturated with deionized water, in the bottom of a petri dish and covering the filter paper with a perforated sheet of Parafilm. Approximately 10 μl of 2 μM CRIA, diluted in Buffer B, was placed in the hydrated chamber and allowed to polymerize and equilibrate overnight. Actin filaments were electrostatically adsorbed to carbon-formvar coated 200 mesh copper electron microscopy grids (Ted Pella, Redding, CA), washed in Buffer B, and coated with heavy metal by brief exposure to 2% uranyl acetate. This technique approximates well the shape and size of actin filaments analyzed in PAF experiments and minimizes disturbance of the sample because no pipetting steps are required. Negatively stained actin filaments were visualized at 5000x on a transmission electron microscope (model JEM-1200EX; JEOL Ltd., Tokyo, Japan) with an accelerating voltage of 80 kV. Photographic negatives were digitized by scanning into a Macintosh G3 computer, and the lengths of 100 actin filaments were measured using macros developed for NIH Image. Actin filament

distributions and statistics were analyzed using the statistical toolbox available for the computational software package Matlab.

RESULTS

Synthesis of caged resorufin actin

CR was synthesized and its photoactivation properties investigated. The chemical linkage that binds the caging group and resorufin fluorophore is extremely light sensitive, especially to UV wavelengths, which cleave the caging group from the fluorophore, releasing its fluorescence. Photoactivation of CR with 365 nm light red-shifts the peak excitation wavelength (Fig. 3-1a), consistent with the absorbance spectra published by Theriot and Mitchison [8]. The peak at 450 nm corresponds to the absorbance of caged resorufin, and 577 nm is the excitation peak of the uncaged resorufin fluorophore.

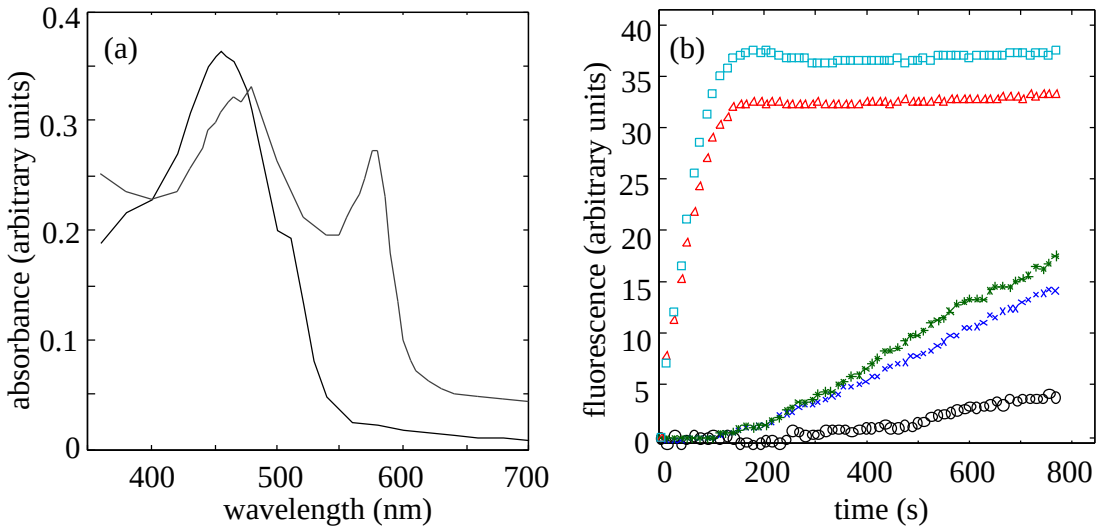

Fig. 3-1. *Caged resorufin actin fluorescence and polymerization properties*. (a) Caged resorufin (—) has an excitation peak at 450 nm, but exposure to UV light at 365 nm uncages resorufin (—) unleashing its native peak fluorescence at 577 nm. (b) CR G- (*) and F-actin (□) nucleation and polymerization in the presence of equimolar pyrene-actin (1 μM) is similar to that of unlabeled G- (×) and F-actin (△). *De novo* nucleation of 1 μM pyrene-actin without additional actin proceeds slower (○).

CR-actin is polymerization competent, and rivals rates of unlabeled actin polymerization (Fig. 3-1b). The rate of nucleation, lag time, and steady state value for CR-actin and unlabeled actin polymerized in the presence of 1 μM pyrene actin are similar. Upon addition of CR-actin or unlabeled actin filament seeds, the lag phase of polymerization is eliminated. The rate of pyrene-actin assembly on CR-actin filament nuclei, dominated by addition at the barbed end, is computed to be 1.42×10^{12} monomers/s, and is nearly identical to the rate of pyrene monomer addition onto unlabeled actin filament seeds at 1.41×10^{12} monomers/s.

BSA coating optimization

In order to control for potential actin binding to the glass microcapillary tube surface, a coating of BSA was applied prior to purified actin solution loading. Bound actin was separated from the BSA coating by SDS-PAGE and quantitated using a linear standard of

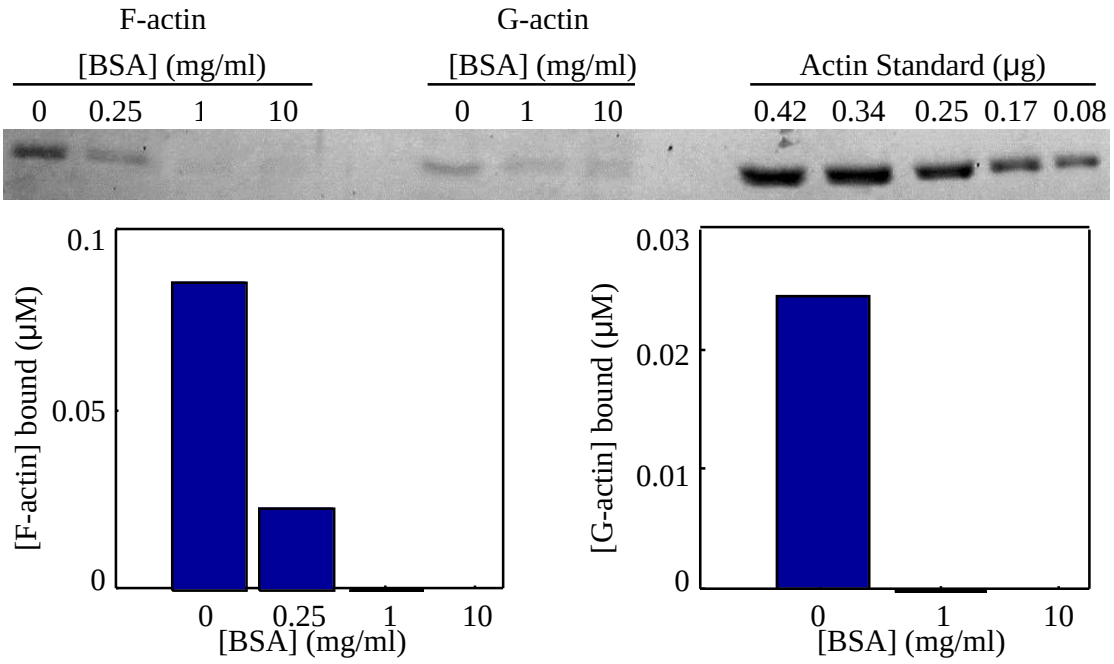

Fig 3-2. *Actin binding to BSA coated glass surfaces*. Quantitation of actin bound to BSA coated glass surfaces by SDS-PAGE reveals that 1 mg/ml BSA eliminates actin-glass interactions (< 80 ng).

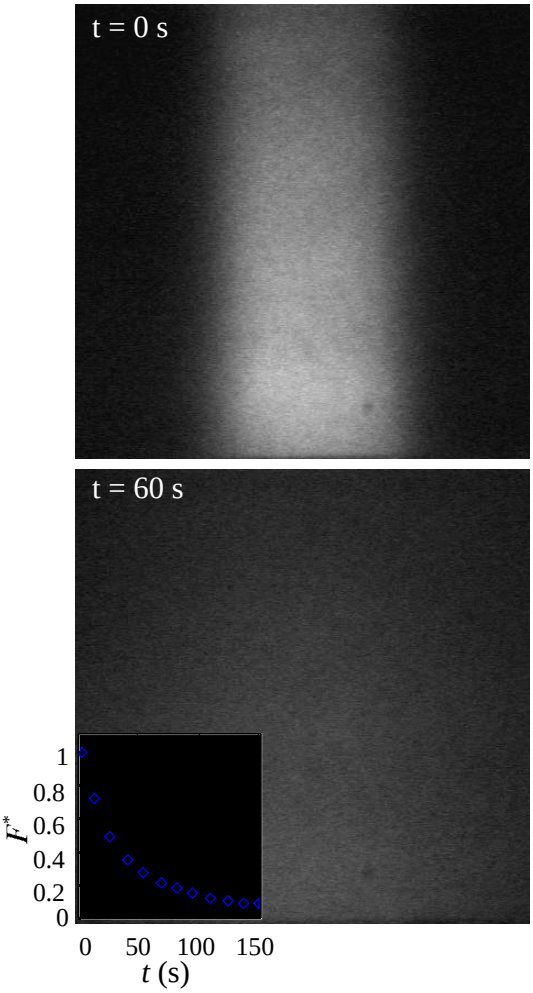

Fig. 3-3. *Actin monomer diffusion from a wide photoactivated band*. Purified G-CR-actin diffuses from wide photoactivated bands rapidly, as evidenced by the complete fluorescent decay after one minute. Bar = 50 μm.

actin (Fig. 3-2). The optimal BSA coating concentration was 1 mg/ml, because at this concentration actin was not detected adherent to the glass surface by SDS-PAGE (< 1% of total actin). Higher concentrations of BSA resulted in aggregates that locally displaced the actin solution in the microcapillary tubes, while lower coating concentrations bound significant amounts of both G- and F-actin.

Actin monomer diffusion

PAF experiments with unpolymerized CR-actin estimate D_m, the diffusivity of actin monomer. G-actin diffuses from the fluorescent region on the order of seconds, and the entire photoactivated band is uniformly dispersed minutes after photoactivation (Fig. 3-3). This behavior is consistent with the short time scale predicted for monomer diffusion from a photoactivated band (Fig. 2-4). Tardy Model analysis of the fluorescence decay estimates the mobility of CR-actin monomer in low salt (Buffer A), aqueous solution at $D_m = 56 \pm 20$ μm^2/s. This measurement agrees with published values by other investigators from $D_m = 49 - 72$ μm^{2}s^{-1} [28, 35].

Actin filament diffusion and turnover

Narrow (30 μm) photoactivated bands decay with time scales for actin filament diffusion and turnover of the same order of magnitude ($\tau_{D_f} \sim \tau_t$). As predicted, narrow photoactivated bands simultaneously broaden and decay (Fig. 3-5). Analysis of narrow photoactivated band experiments with the Tardy Model reveals a nondimensional relationship between centerline fluorescence decay (F^*) and photoactivated band width (ω^*) that approximates the theoretical diffusion and turnover regime developed in Chapter II. This implies that actin filament diffusion and turnover are occurring simultaneously in narrow photoactivated bands.

After the initial decay due to monomer diffusion, the long-time nondimensional fluorescence decay is fit by an exponential ($R^2 = 0.75 \pm 0.02$), according to the theory of the simplified Tardy Model (see methods, Chapter II). The simplified Tardy Model estimates the actin polymer fraction and characteristic decay time ($PF = 0.68 \pm 0.02$; $\tau = 3.1 \pm 0.3$ hrs; $n = 31$). The polymer fraction is also a measure of the critical concentration of ATP-CR-actin, $C_{c\text{-}ATP} = C_a(1\text{-PF}) = 0.64$ μM, where $C_a = 2$ μM, the total actin concentration. This value is slightly higher than reported for other labeled and unlabeled actins, most likely due to a combination of the low concentration of total actin used in these experiments,

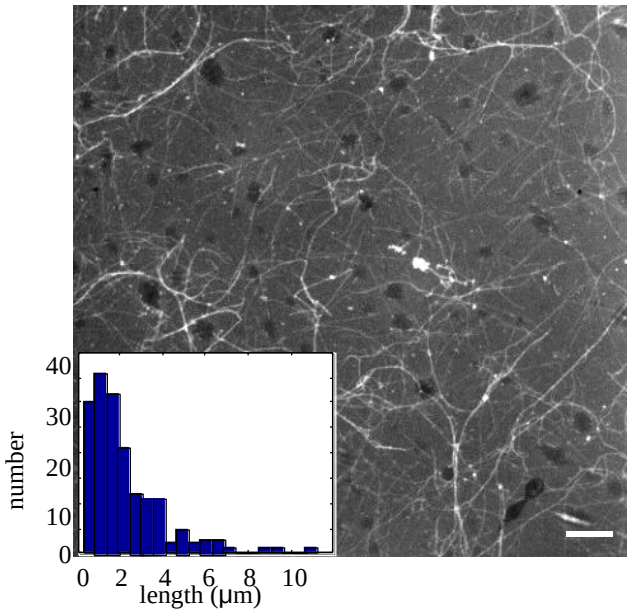

Fig. 3-4. *Negatively stained purified actin filaments*. Electron micrographs of polymerized actin were used to measure 100 actin filaments and compute the average filament length, L_{avg}. Bar = 1 μm. *Inset*: Histogram of actin filament lengths.

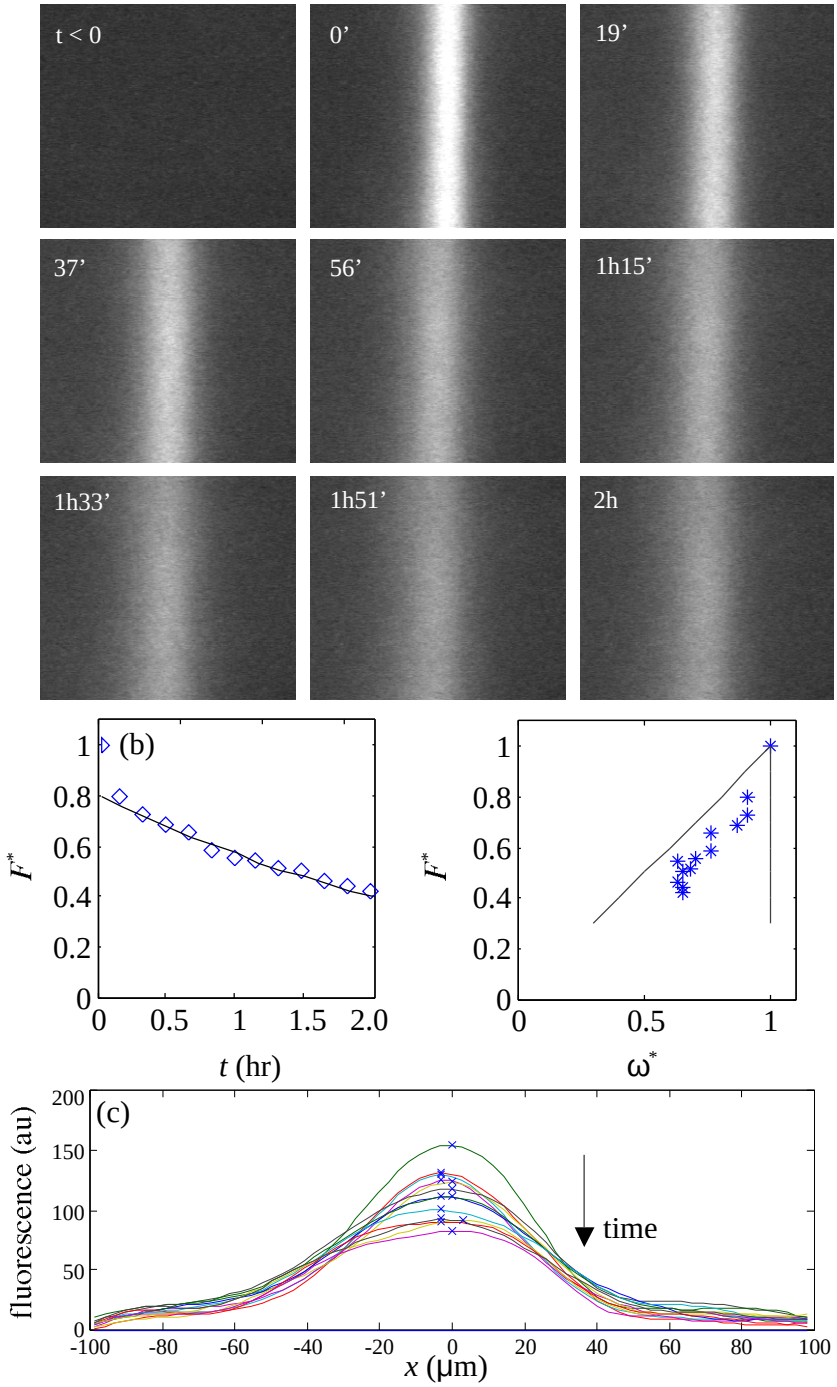

Fig. 3-5. *Narrow photoactivated band actin dynamics.* (a) Uncaged CR-actin in narrow photoactivated bands simultaneously decays and broadens over time. (b) The simplified Tardy Model describes the fluorescenct decay at long times accurately. Nondimensional analysis provides a relationship between centerline fluorescence decay and photoactivated band width that follows the predicted relationships defined in Chapter II. (c) Narrow photoactivated band spatial profiles broaden over time.

approaching the critical concentration of ATP-actin at the pointed end, and effects of CR labeling. As an estimate of actin filament diffusion characteristics, average filament lengths were measured at L_{avg} = 2.3 ± 0.3 μm from electron micrographs of negatively stained actin filaments (Fig. 3-4), corresponding to $D_f \approx 0.16$ μm^2/s calculated from Eq. 2.11. The distribution of actin filament lengths is skewed towards shorter filaments, consistent with measured distributions in other studies and by different methods [36].

Actin filament turnover

The time scale for wide (230 μm) photoactivated bands predicts actin filament diffusion times to be orders of magnitude longer than actin filament turnover ($\tau_{D_f} >> \tau_t$). Therefore, wide photoactivated bands theoretically decay without broadening of the photoactivated band, consistent with an actin filament turnover-mediated fluorescence evolution. PAF experiments with wide bands validate this theory: the fluorescence contained initially within the photoactivated band decays without an increase in band width (Fig. 3-6). Analysis of the relationship between F^* and ω^* produces a curve consistent with the predicted actin filament turnover regime. This implies that wide photoactivated bands decay predominately due to the cyclic turnover of actin filaments.

Analysis of the time-dependent centerline fluorescence decay with the simplified Tardy Model and a best-fit exponential curve (R^2 = 0.75 ± 0.05) estimates the lifetime of purified actin filaments at τ_t = 7.8 ± 1.5 hours and a polymer fraction of PF = 0.63 ± 0.07. The critical concentration for ATP-CR-actin is calculated to be $C_{c\text{-}ATP}$ = 0.74 μM. Electron micrographs of negatively stained CR-actin filaments in wide photoactivated band experiments were similar to those in narrow band experiments (Fig. 3-4). The average actin filament length was measured at L_{avg} = 2.6 ± 0.2 μm. Assuming a treadmilling model of actin filament turnover, the kinetic dissociation rate of ADP-actin

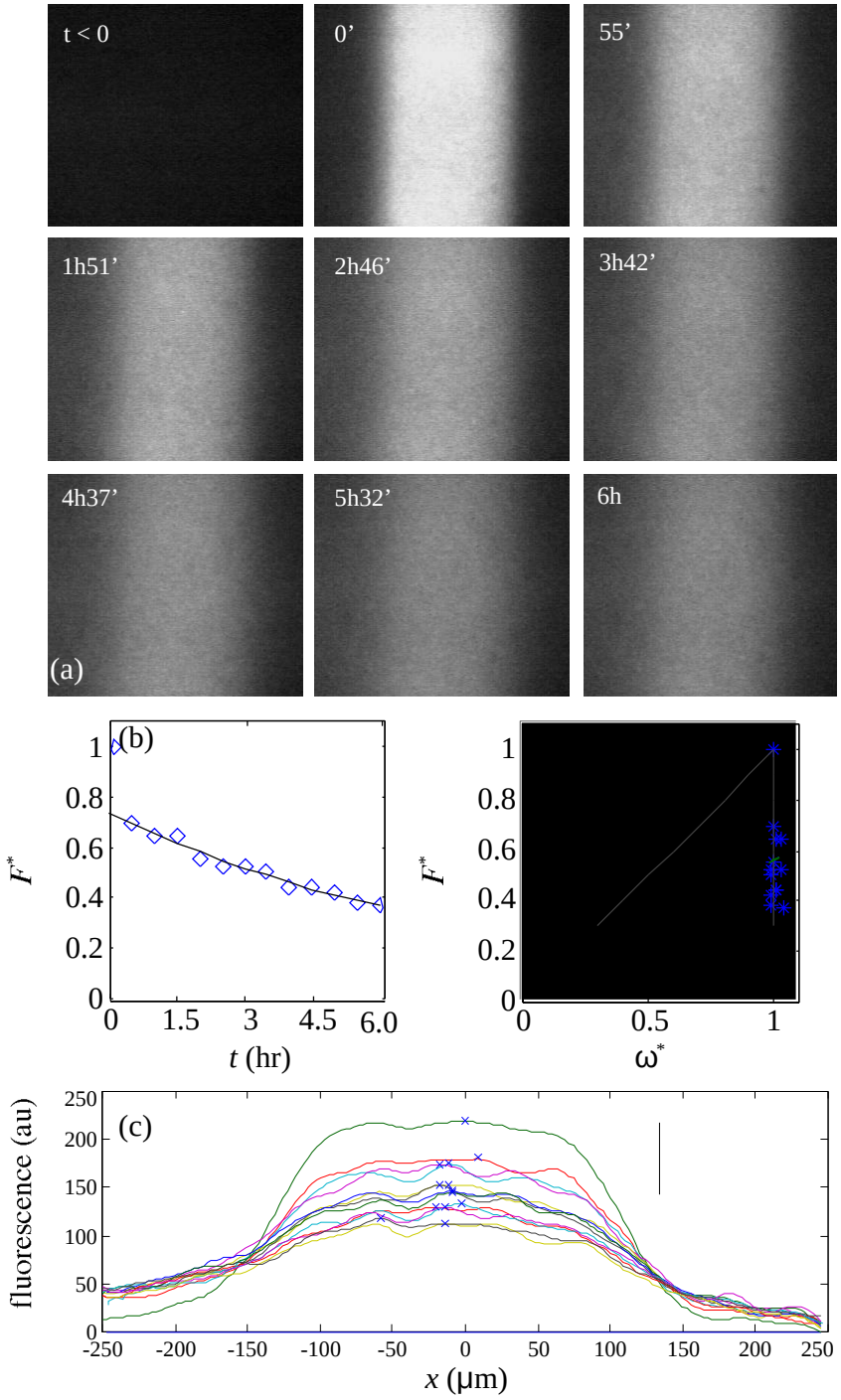

Fig. 3-6. *Wide photoactivated band actin dynamics.* (a) Uncaged CR-actin in wide photoactivated bands decays over time without broadening. (b) Nondimensional analysis reveals a relationship that follows the theoretical decay for pure actin filament turnover as defined in Chapter II. (c) Wide photoactivated band spatial profiles remain at a fixed width as they decay.

at the pointed actin filament end is calculated as K_{pD}^{-} = 0.034 s^{-1}, in close approximation to the published value by Janmey and colleagues of K_{pD}^{-} = 0.03 s^{-1} [37].

Stabilizing actin filaments in wide photoactivated bands

Stabilizing actin filaments against depolymerization is predicted to halt actin filament turnover, and therefore eliminate the fluorescence decay in a wide photoactivated band. Phallacidin, a protein extracted from the deadly mushroom *Amanita phalloides*, binds to the sides of actin filaments and stabilizes them against disassembly [24]. It differs from its more commonly used analog, phalloidin, by just two amino acids [38]. Phallacidin has nM affinity for actin filaments and associates with actin filament subunits in a 1:1 stoichiometry, but is unable to bind to G-actin, [25]. In experiments that include equimolar amounts of phallacidin with actin, wide photoactivated bands of actin do not decay (Fig. 3-7), and have extremely long characteristic time constants (τ = 66.5 ± 26.9 hrs). Phallacidin also increases the amount of actin polymerized (PF = 0.87 ± 0.08) and the average filament length (L_{avg} = 3.6 ± 0.5 μm). Increased polymerization of actin and decreased filament turnover are consistent with the stabilizing effect of phallacidin-F-actin subunit complexes, which reduce the critical

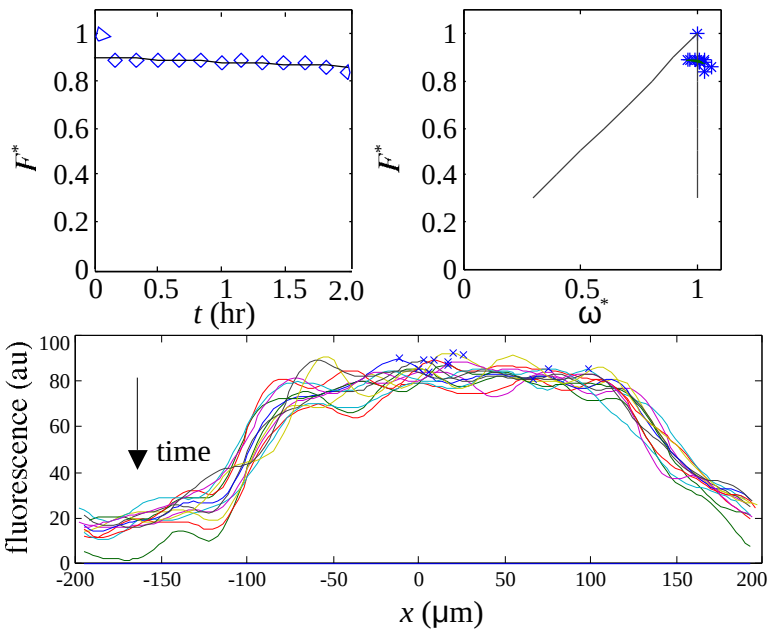

Fig. 3-7. *Phallacidin-actin dynamics in wide photoactivated bands.* (a) The rate of fluorescent decay is greatly diminished, due to the elimination of actin filament turnover with phallacidin. (b) Spatial profiles of wide bands with phallacidin do not broaden over time.

concentration of polymerization at both filament ends to nearly zero [24].

Crosslinking actin filaments in narrow photoactivated bands

Crosslinked actin gels should theoretically eliminate actin filament diffusion, slowing the fluorescence decay of narrow photoactivated bands to levels observed for pure actin filament turnover in wide photoactivated bands. ABP-120 from the slime mold *Dictyostelium discoidium* is a potent actin filament crosslinking protein *in vitro*, and essential to *Dictyostelium* cortical actin network structure [39]. ABP-120 self-associates to form 240 kDa dimers in solution, in which each constituent ABP-120 molecule binds one actin filament creating a three-dimensional gel, analogous to the function of the filamin family of proteins in humans [40]. Narrow photoactivated bands in the presence of ABP-120 exhibit a characteristic fluorescence decay time constant (τ_t = 12.1 ± 2.8 hrs) that is longer than measurements in wide photoactivated bands, and do not broaden (Figure 3-8). These results implicate filament turnover as the dominant mechanism underlying fluorescence decay, and that filament crosslinking slows filament turnover to a significantly. The polymer fraction slightly increases in the presence of ABP-120 (PF = 0.85 ± 0.02), but the average actin

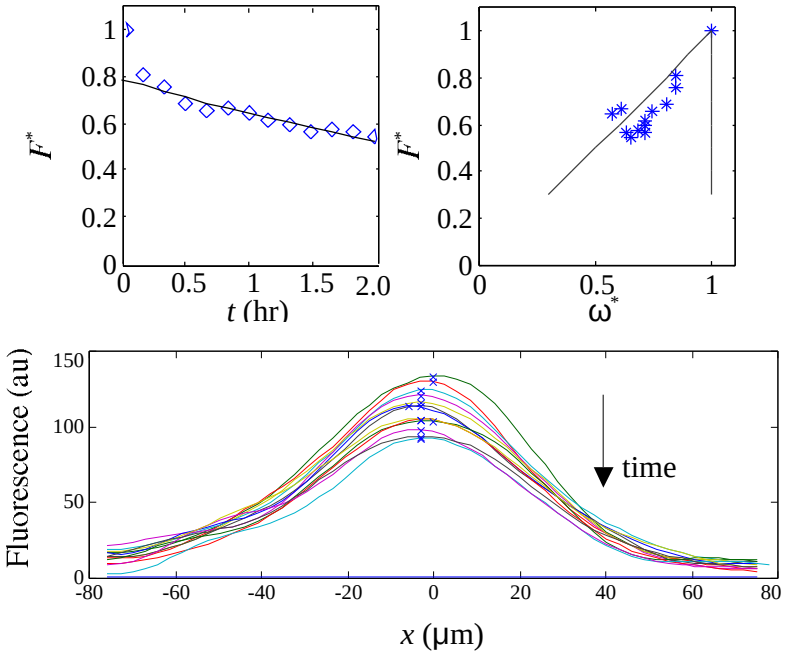

Fig. 3-8. *ABP-120-actin dynamics in narrow photoactivated bands*. (a) The rate of fluorescent decay is reduced, and diffusion eliminated, upon actin gel formation. (b) Spatial profiles of narrow bands with ABP-120 do not broaden over time.

filament length does not (L_{avg} = 2.4 ± 0.2), indicating that an increased number of actin filaments are produced, consistent with published reports that addition of filamin-A to purified actin networks an results in an increased number of small actin filaments [41].

DISCUSSION

For filaments of approximately the same length, the characteristic fluorescence decay time in wide photoactivated bands is ~three-fold longer than narrow bands, because actin filament diffusion is markedly slowed with increased photoactivated band widths. These results, along with the observation that narrow, but not wide, photoactivated bands of actin broaden over time, validates the theory presented in Chapter II and confirms that the separation of actin filament diffusion and turnover is possible if the width of the photoactivated band is changed. From measurements of filament turnover in wide bands, the calculated kinetic rate at which F-actin subunits dissociate from pointed ends *in vitro* is consistent with the lowest values measured by other investigators on purified actin preparations.

Formation of a crosslinked actin gel should theoretically hinder filament diffusion from photoactivated bands. As predicted, narrow photoactivated band broadening was eliminated in experiments combining purified actin and ABP-120. Unexpectedly, crosslinked actin gels also exhibited decreased rates of filament turnover. While the exact nature of binding between ABP-120 and actin is unknown, ABP-120 may overlap adjacent F-actin subunits and link them together to stabilize the filament. If this occurs at the end of the actin filament, stabilization by ABP-120 would act as a capping protein and reduce F-actin subunit dissociation, explaining the observed decrease in filament turnover rates. Other mechanisms by which ABP-120-mediated filament crosslinking could increase the lifetime of actin filaments are by reducing the hydrolysis rate of ATP-F-actin subunits or by altering the normal helical conformation of the filament, possibly by influencing the twist of the filament.

Phallacidin is known to reduce the dissociation rate of F-actin subunits from filaments, stabilizing them against depolymerization and eliminating filament treadmilling. Wide photoactivated bands, which decay exclusively due to filament turnover, do not decay in the presence of equimolar amounts of phallacidin, verifying the stabilizing effect that phallacidin exhibits on actin filaments. By stabilizing actin filaments against depolymerization, phallacidin reduces the critical concentration significantly causing filaments to polymerize more extensively. PAF experiments support this mechanism as evidenced by the marked increase in the actin polymer fraction and average filament length.

This novel system allows for a noninvasive measurement of actin filament dynamics at a true steady state in purified actin networks. It also is highly suitable for examining the effects of purified actin regulatory proteins on actin filament diffusion and turnover in order to validate or reform the mechanisms by which these proteins alter actin dynamics. Candidate actin regulatory proteins to analyze with this system include CapZ (barbed end capping), gelsolin (severing and barbed end capping), ADF/cofilin (accelerated depolymerization and severing), filamin (actin filament crosslinking), and the Arp2/3 complex (nucleation and pointed end capping). Synergy between different actin-regulatory proteins is likely to be important to achieve the filament cycling rates observed in cells. By understanding the individual mechanisms of regulatory proteins on actin dynamics, reconstitution of actin networks with purified proteins that model cellular behavior may be possible.

REFERENCES

1. McGrath JL: Actin dynamics in the cell cytoplasm and the role of actin associated proteins [PhD]. Harvard - MIT; 1998.

2. Pollard TD: Rate constants for the reactions of ATP- and ADP-actin with the ends of actin filaments. J Cell Biol 1986; 103(6 Pt 2): 2747-54.

3. Selve N, Wegner A: Rate of treadmilling of actin filaments in vitro. J Mol Biol 1986; 187(4): 627-31.

4. Wegner A: Head to tail polymerization of actin. J Mol Biol 1976; 108(1): 139-50.

5. Korn ED, Carlier MF, Pantaloni D: Actin polymerization and ATP hydrolysis. Science 1987; 238(4827): 638-44.

6. McGrath JL, Osborn EA, Hartwig JH, Dewey CF, Jr.: A mechanistic model of the actin cycle in cells. Annals of Biomedical Engineering 2001; manuscript in progress.

7. Theriot JA, Mitchison TJ: Comparison of actin and cell surface dynamics in motile fibroblasts. J Cell Biol 1992; 119(2): 367-77.

8. Theriot JA, Mitchison TJ: Actin microfilament dynamics in locomoting cells. Nature 1991; 352(6331): 126-31.

9. Wang YL: Exchange of actin subunits at the leading edge of living fibroblasts: possible role of treadmilling. J Cell Biol 1985; 101(2): 597-602.

10. McGrath JL, Osborn EA, Tardy YS, Dewey CF, Jr., Hartwig JH: Regulation of the actin cycle in vivo by actin filament severing. Proc Natl Acad Sci U S A 2000; 97(12): 6532-6537.

11. McGrath JL, Tardy Y, Dewey CF, Jr., Meister JJ, Hartwig JH: Simultaneous measurements of actin filament turnover, filament fraction, and monomer diffusion in endothelial cells. Biophys J 1998; 75(4): 2070-8.

12. Kreis TE, Geiger B, Schlessinger J: Mobility of microinjected rhodamine actin within living chicken gizzard cells determined by fluorescence photobleaching recovery. Cell 1982; 29(3): 835-45.

13. Spudich JA, Watt S: The regulation of rabbit skeletal muscle contraction. I. Biochemical studies of the interaction of the tropomyosin-troponin complex with actin and the proteolytic fragments of myosin. J Biol Chem 1971; 246(15): 4866-71.

14. MacLean-Fletcher S, Pollard TD: Identification of a factor in conventional muscle actin preparations which inhibits actin filament self-association. Biochem Biophys Res Commun 1980; 96(1): 18-27.

15. Casella JF, Barron-Casella EA, Torres MA: Quantitation of Cap Z in conventional actin preparations and methods for further purification of actin. Cell Motil Cytoskeleton 1995; 30(2): 164-70.

16. Caldwell JE, Heiss SG, Mermall V, Cooper JA: Effects of CapZ, an actin capping protein of muscle, on the polymerization of actin. Biochemistry 1989; 28(21): 8506-14.

17. Walker JW, Reid GP, Trentham DR: Synthesis and properties of caged nucleotides. Methods Enzymol 1989; 172: 288-301.

18. dos Remedios CG, Miki M, Barden JA: Fluorescence resonance energy transfer measurements of distances in actin and myosin. A critical evaluation. J Muscle Res Cell Motil 1987; 8(2): 97-117.

19. Kouyama T, Mihashi K: Fluorimetry study of N-(1-pyrenyl)iodoacetamide-labelled F-actin. Local structural change of actin protomer both on polymerization and on binding of heavy meromyosin. Eur J Biochem 1981; 114(1): 33-8.

20. Wang YL, Taylor DL: Preparation and characterization of a new molecular cytochemical probe: 5-iodoacetamidofluorescein-labeled actin. J Histochem Cytochem 1980; 28(11): 1198-206.

21. Miki M, O'Donoghue SI, Dos Remedios CG: Structure of actin observed by fluorescence resonance energy transfer spectroscopy. J Muscle Res Cell Motil 1992; 13(2): 132-45.

22. Betcher-Lange SL, Lehrer SS: Pyrene excimer fluorescence in rabbit skeletal alphaalphatropomyosin labeled with N-(1-pyrene)maleimide. A probe of sulfhydryl proximity and local chain separation. J Biol Chem 1978; 253(11): 3757-60.

23. McGrath JL, Hartwig JH, Tardy Y, Dewey CF, Jr.: Measuring actin dynamics in endothelial cells. Microsc Res Tech 1998; 43(5): 385-94.

24. Coluccio LM, Tilney LG: Phalloidin enhances actin assembly by preventing monomer dissociation. J Cell Biol 1984; 99(2): 529-35.

25. Wieland T, Faulstich H: Amatoxins, phallotoxins, phallolysin, and antamanide: the biologically active components of poisonous Amanita mushrooms. CRC Crit Rev Biochem 1978; 5(3): 185-260.

26. MacLean-Fletcher SD, Pollard TD: Viscometric analysis of the gelation of Acanthamoeba extracts and purification of two gelation factors. J Cell Biol 1980; 85(2): 414-28.

27. Tardy Y, McGrath JL, Hartwig JH, Dewey CF: Interpreting photoactivated fluorescence microscopy measurements of steady-state actin dynamics. Biophys J 1995; 69(5): 1674-82.

28. Lanni F, Ware BR: Detection and characterization of actin monomers, oligomers, and filaments in solution by measurement of fluorescence photobleaching recovery [published erratum appears in Biophys J 1989 Jul;56(1):following 222]. Biophys J 1984; 46(1): 97-110.

29. Ishihara A, Gee K, Schwartz S, Jacobson K, Lee J: Photoactivation of caged compounds in single living cells: an application to the study of cell locomotion. Biotechniques 1997; 23(2): 268-74.

30. Vigers GP, Coue M, McIntosh JR: Fluorescent microtubules break up under illumination. J Cell Biol 1988; 107(3): 1011-24.

31. Simon JR, Gough A, Urbanik E, et al.: Analysis of rhodamine and fluorescein-labeled F-actin diffusion in vitro by fluorescence photobleaching recovery. Biophys J 1988; 54(5): 801-15.

32. Axelrod D: Cell surface heating during fluorescence photobleaching recovery experiments. Biophys J 1977; 18(1): 129-31.

33. Carlier MF, Pantaloni D, Korn ED: Evidence for an ATP cap at the ends of actin filaments and its regulation of the F-actin steady state. J Biol Chem 1984; 259(16): 9983-6.

34. Bonder EM, Fishkind DJ, Mooseker MS: Direct measurement of critical concentrations and assembly rate constants at the two ends of an actin filament. Cell 1983; 34(2): 491-501.

35. Tait JF, Frieden C: Polymerization and gelation of actin studied by fluorescence photobleaching recovery. Biochemistry 1982; 21(15): 3666-74.

36. Burlacu S, Janmey PA, Borejdo J: Distribution of actin filament lengths measured by fluorescence microscopy. Am J Physiol 1992; 262(3 Pt 1): C569-77.

37. Janmey PA, Stossel TP: Kinetics of actin monomer exchange at the slow growing ends of actin filaments and their relation to the elongation of filaments shortened by gelsolin. J Muscle Res Cell Motil 1986; 7(5): 446-54.

38. Wieland T: Phallotoxins. New York: Springer-Verlag, 1986.

39. Condeelis J, Vahey M, Carboni JM, DeMey J, Ogihara S: Properties of the 120,000- and 95,000-dalton actin-binding proteins from Dictyostelium discoideum and their possible functions in assembling the cytoplasmic matrix. J Cell Biol 1984; 99(1 Pt 2): 119s-126s.

40. Dubreuil RR: Structure and evolution of the actin crosslinking proteins. Bioessays 1991; 13(5): 219-26.

41. Hartwig JH, Tyler J, Stossel TP: Actin-binding protein promotes the bipolar and perpendicular branching of actin filaments. J Cell Biol 1980; 87(3 Pt 1): 841-8.

Chapter IV

Actin Dynamics and Regulation in Endothelial Cells

In a mechanically wounded monolayer, endothelial cells crawl at different speeds and exhibit altered actin dynamics depending on their proximity to the wound edge [1]. Slow-moving, confluent cells far from the wound edge have long filament lifetimes and high polymer content. Subconfluent cells crawling freely in the wound are more motile, polymerize approximately half as much actin, and cycle F-actin subunits ~5-fold more quickly than confluent cells (Table 1-1). A mechanism to explain the strong correlations observed between endothelial cell speed, polymer fraction, and filament turnover (Fig. 1-7) is required to bridge the molecular actions of cytoplasmic proteins with global cellular shape change.

Increased actin filament turnover is consistent with mechanisms attributed to the actin depolymerization factor (ADF) and cofilin family of regulatory proteins [2]. Kinetic analysis of actin filament dynamics *in vitro* reveals that accelerated actin filament turnover by ADF/cofilin will produce net filament depolymerization in the presence of sequestering proteins [3]. Mechanisms attributed to other actin binding proteins could also account for the changes observed in endothelial cell actin dynamics as they alter speed. In order to determine the effect of different proteins on actin dynamics, additional parameters describing the state of actin in endothelial cells are required: the number of uncapped barbed and pointed ends, the average filament length, and the total number of cytoskeletal filaments. Determination of these parameters will allow prediction of mechanisms that regulate endothelial cell motility.

METHODS

Cell culture

Primary cultures of bovine aortic endothelial cells (BAECs) used in these experiments were a gift of Dr. Michael A. Gimbrone, Jr. (Vascular Research Division, Brigham and Women's Hospital, Boston, MA). BAECs were grown on Falcon® 100 mm vacuum gas plasma treated petri dishes (Becton Dickinson, Franklin Lakes, NJ) with complete DMEM (low glucose Dulbecco's Modified Eagle's Medium, 10% calf serum, 100 U/ml penicillin/streptomycin, and 2 mM L-glutamine) and placed in a humidified incubator set to 37°C and 5% CO_2. Confluent BAEC monolayers were passaged 1:4 with 0.05% trypsin/ 0.02% EDTA for culture propagation, and only BAECs between subculture 5 and 15 were used for experiments.

Actin assembly measurements

Borosilicate glass test tubes (Kimble/Kontes, Vineland, NJ) were cleaned, autoclaved, and coated with a 0.1% gelatin solution (Sigma, St. Louis, MO). BAECs suspended in LB culture media (Liebovitz's L-15 Media, 10% calf serum, 100 U/ml penicillin/streptomycin, and 2 mM L-glutamine) were plated in the glass tubes at room temperature under constant rotation in a laminar flow hood for 2 hours. After cell seeding, the glass tubes were removed from the rotation device, LB culture media was replaced with complete DMEM, and the BAECs were transferred to a humidified incubator at 37°C and 5% CO_2 for subsequent culture. BAECs were cultured to either ~30% or 100% confluence for subconfluent and confluent pyrene actin nucleation assays, respectively. Prior to each experiment, the average BAEC density was measured from at least four digital images captured with a 10x phase contrast objective using macros written for the public domain software NIH Image (v. 1.62; developed at the U.S.

National Institutes of Health and available on the Internet at http://rsb.info.nih.gov/nih-image/).

Measurement of actin monomer assembly onto uncapped actin filament ends was accomplished using a previously described assay based on introducing trace amounts of pyrene iodacetamide labeled rabbit α-skeletal muscle G-actin (pyrene-actin) into membrane-extracted cells [4]. When incorporated into actin filaments, pyrene-actin is ~25-fold more fluorescent than when unpolymerized. Therefore, monitoring the fluorescence evolution over time, as pyrene-actin monomers add onto exogenous actin filament ends of permeabilized BAECs, estimates the number of actin filament barbed ends available for polymerization. Addition of the barbed end capping agent, cytochalasin B (cytoB), allows determination of the number of uncapped actin filament pointed ends in BAEC actin cytoskeletons [5]. CytoB is a fungal metabolite that binds with nM affinity to the barbed end of actin filaments, inhibiting actin monomer association and dissociation at this site [6].

To access the underlying detergent-insoluble actin cytoskeleton, BAECs were washed 3x with serum-free LB culture media, and cell membranes were removed by the addition of PHEM permeabilization/nucleation buffer (60 mM PIPES, 25 mM HEPES, 10 mM EGTA, 2 mM MgCl, 0.1% Triton X-100, 2 μM phallacidin, 150 mM KCl, pH 6.9) for 2 minutes at 37°C. Addition of 1 μM pyrene actin to exposed BAEC actin cytoskeletons, followed by brief vortexing, initiated actin assembly experiments. Pyrene actin fluorescence evolution was monitored for 10 minutes (Ex. 366 nm, Em. 386 nm) with a Fluoromax-2® fluorescence spectrometer (Jobin Yvon Inc., Edison, NJ). Final fluorescence measurements for each test tube were performed 24 hours after completion of the actin assembly assay. Experiments were repeated in the presence of 2 μM cytoB to measure cellular pointed end assembly. Controls without BAEC insured that pyrene-actin nucleation was cytoskeleton specific, while those with 1 to 10% calf serum proved that nucleation was not due to effects of residual serum proteins from the culture media.

The number of barbed and pointed ends per cell was determined according to the number of cells contributing to the measured fluorescence, the initial rate of change of the fluorescence profile, and the published kinetic rates for actin monomer addition at each filament end. From cell density measurements, the total number of cells illuminated by the excitation fluorescence (n_{cells}), and therefore contributing to fluorescence measurements, was determined by multiplying the cell surface densities by the illuminated are of the glass tube (A_{surf} = 1.57 cm^2). The initial rate of change of fluorescence was determined by calculating the slope of a linear fit using least-squares regression to the first 150 seconds of the fluorescence curve. Given the initial rate of pyrene actin assembly ($\dot{F}$), the initial (F_i) and final fluorescence (F_f) values, the published rates of actin assembly at the two filament ends, and n_{cells}, the number of uncapped actin filament ends per endothelial cell can be calculated (n_x).

$$n_x = \left(1 \times 10^{-12}\right) \frac{\left(\dot{F}\right)\left(V\right)\left(N_A\right)}{\left(K_{xT}^{+}\right)\left(F_f - F_i\right)\left(n_{cells}\right)} \tag{4.1}$$

In this equation, V is the total volume of fluid per test tube in μl, and N_A is Avagadro's Constant. The subscript x is replaced by either p or b in order to designate the pointed or barbed filament end, respectively. Kinetic rates of actin assembly at the barbed and pointed ends were taken from published values to be K_{bT}^{+} = 11.6 $\mu M^{-1}s^{-1}$ and K_{pT}^{+} = 1.3 $\mu M^{-1}s^{-1}$, respectively [7].

Actin quantitation

Confluent or ~30% subconfluent BAECs, corresponding to the fastest and slowest cells in wound healing experiments (Fig 1-6), were lysed while adherent to 100 mm petri dishes by covering the cells with a minimal amount of Triton lysis buffer (1 mM EDTA, 150 mM NaCl, 50 mM Tris, 1% Triton X-100, 200 mM PMSF, 0.1 mg aprotinin, 0.1 mg leupeptin, 0.1 mg benzamide, pH 7.4). Cell lysates were collected by scraping. Protein remaining adherent to petri dishes was solubilized with a small volume of lysis buffer

containing 2% sodium dodecyl sulfate (SDS) to assay for completeness of protein recovery. The total protein for whole cell lysate samples was determined with a Pierce BCA protein assay (Pierce Chemical Co., Rockford, IL). Triton soluble and insoluble cell fractions were separated by centrifugation at 350,000 x g for 30 min at 37˚C. The total protein loaded for the two phenotypes was matched for SDS–polyacrylamide gel electrophoresis (SDS-PAGE). Commassie Brilliant Blue (CBB) stained gels were digitized and quantitated against a linear standard of purified actin using the densitometric features of NIH Image.

Cofilin quantitation

The same subconfluent and confluent BAECs fractionated into Triton soluble and insoluble fractions were used to determine the cofilin content. As before, samples were adjusted to match total protein, and then proteins were separated by SDS-PAGE. Proteins were then transferred to PVDF membranes for antibody probing by using a wet transfer apparatus (BioRad Laboratories, Hercules, CA) filled with transfer buffer (25 mM TRIS-HCl, 192 mM glycine, 0.1% SDS, 20% methanol, pH 8.3). Membranes were blocked overnight at 4˚C under constant rocking in blocking buffer (1.5 mM $NaH_2PO_4 \cdot H_2O$, 8.1 mM Na_2HPO_4, 145 mM NaCl, 0.05% Tween-20, 5% nonfat dry milk, pH 7.4) and probed with rabbit polyclonal antisera developed against human recombinant cofilin (1:1000). Cofilin detection was accomplished using a horseradish peroxidase-conjugated goat anti-rabbit secondary antibody (1:5000), and incubation in Pierce ECL chemiluminescence reagent, followed by brief exposure to Kodak Biomax® MR photographic film (Eastman Kodak, Rochester, NY). Cofilin levels from film images were quantitated using NIH Image in a similar manner to actin levels.

RESULTS

Actin polymer fraction

PAF measures the actin polymer fraction for a single endothelial cell, but separation of detergent soluble and insoluble fractions from fractionated lysates of multiple cells is the standard technique to determine polymerized and unpolymerized actin [8]. From SDS-PAGE, the concentration of filamentous and monomeric actin can be estimated (Fig 4-1). Densitometric measurements after CBB staining indicates that 58 ± 6% of endothelial actin is Triton insoluble in the confluent phenotype and 46 ± 6% is Triton insoluble in the subconfluent phenotype ($n = 3$; $p < 0.05$), a modest agreement with the photoactivation of fluorescence estimates in intact, individual cells. Therefore, the trends for actin polymer fraction observed in PAF experiments on BAECs correlate positively with this biochemical data. Although the total protein content in both phenotypes remained at ~60 pg/cell, pooling the detergent soluble and insoluble cellular fractions reveals that confluent BAECs have slightly less total actin (78.5 ± 16.7 μM) than subconfluent endothelial cells (101 ± 14 μM), assuming a 2 pl cytoplasmic volume.

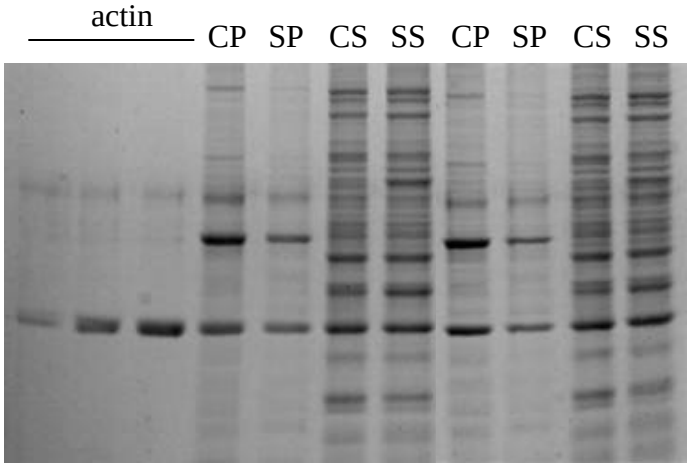

Fig. 4-1. *Actin monomer and filament concentration in BAECs*. Actin fractionated into detergent soluble (S = supernatant) and insoluble (P = pellet) cytoskeletal fractions allows quantitation of the partitioning of cytoplasmic actin. Subconfluent BAECs have less actin incorporated into filaments (SP) than confluent cells (CP). CP = confluent pellet; CS = confluent supernatant; SP = subconfluent pellet; and SS = subconfluent supernatant. The arrow indicates the bands corresponding to the 42 kDa actin molecule.

Actin filament end counts

In order to examine changes in the distribution and state of actin filaments within the cell cytoskeleton, assays were performed to determine the number of uncapped filament ends in subconfluent and confluent BAECs. In permeabilized BAEC cytoskeleton preparations, subconfluent BAECs nucleate pyrene-actin on their existing filaments ~10-fold faster per cell than confluent BAECs (Fig. 4-2). Subconfluent BAECs are also more sensitive to the barbed end blocking agent cytochalasin B (cytoB), implying that these cells have more rapid-assembly competent barbed ends exposed. Utilizing the published rates of monomer assembly and the difference between nucleation with and without cytoB, subconfluent BAECs have 231,000 ± 86,700 free pointed ends per cell and 59,400 ± 29,100 free barbed ends, while confluent BAECs have 53,800 ± 12,300 free pointed ends per cell and 3,080 ± 1,280 free barbed ends per cell.

Historically the number of free pointed ends has been equated to the total number of actin filaments [5, 9]. Using this assumption, the fraction of barbed ends exposed increases from 5.6 ± 1.6% in confluent cells to 30.8 ± 15.0% in subconfluent cells ($p < 0.01$).

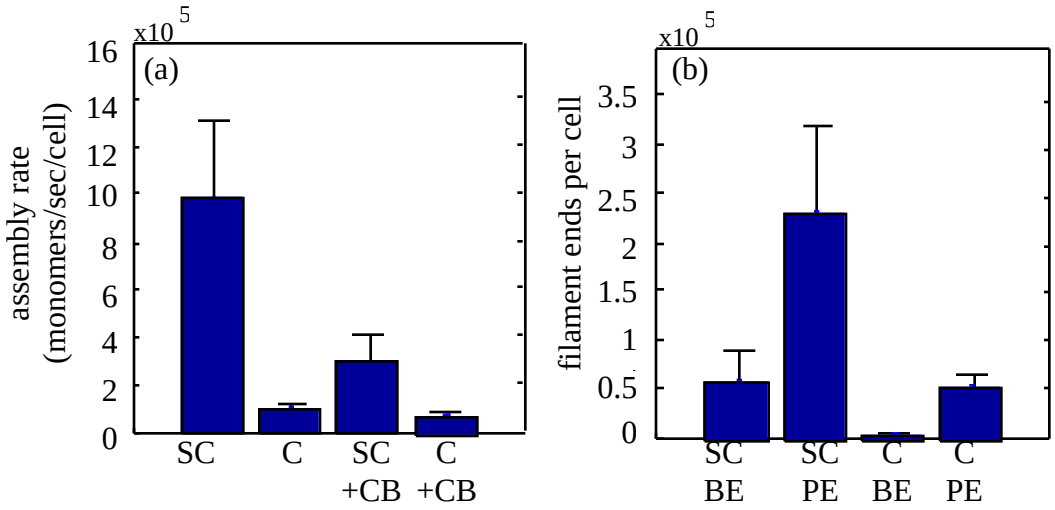

Fig. 4-2. *BAEC actin filament ends.* (a) Pyrene-actin assembles onto permeabilized subconfluent (SC) endothelial cell cytoskeletons ten-fold faster than confluent (C), and this rate is significantly reduced in the presence of cytochalasin B (CB). (b) Subconfluent BAECs have more actin filament ends available for polymerization. BE = barbed end (BE); PE = pointed end.

Given that the Arp2/3 complex can bind to actin filament pointed ends [10], the assumption that all pointed ends are uncapped may underestimate actin filament number in these assays.

Actin filament length

Assuming similar cytoplasmic volumes, the number of actin filaments in each phenotype can be combined with the estimates of total actin content from SDS-PAGE and the polymer fraction from PAF experiments to compute an average filament length. The cytoplasmic volume of an endothelial cell is estimated at ~2 pl, given typical planar dimensions of 40 μm by 20 μm and assuming an average height of ~3 μm based on measurements of surface topography with an atomic force microscope [11]. This is most likely a slight overestimate of the cytoplasmic volume since a portion of this subcellular space will be occupied by organelles, the nucleus, and membrane-bound vesicles. The total actin concentration per cell was measured at ~100 μM by SDS-PAGE for both confluent and subconfluent BAECs. Therefore, the average filament length is ~3 μm for the confluent phenotype and ~0.56 μm for the subconfluent phenotype. As before, if n_f is underestimated due to actin filament pointed end capping by the Arp2/3 complex, the average length will be overestimated. However, slight overestimation of the cytoplasmic volume may counter this effect.

Cofilin content

Western analysis of the same fractions used for actin quantitation reveal that 20.5 ± 5.4% of cytoplasmic cofilin is associated with the Triton insoluble actin cytoskeleton in confluent BAECs, compared to only 11.6 ± 2.7% in subconfluent cells (Fig. 4-3). As regulated by LIM-kinase 1 [12], cofilin in its dephosporylated form is able to bind to F-actin subunits [13, 14], where the affinity of cofilin for ADP-actin (K_d = 0.1 μM) is approximately two orders of magnitude greater than that for actin bound to ATP (K_d = 8

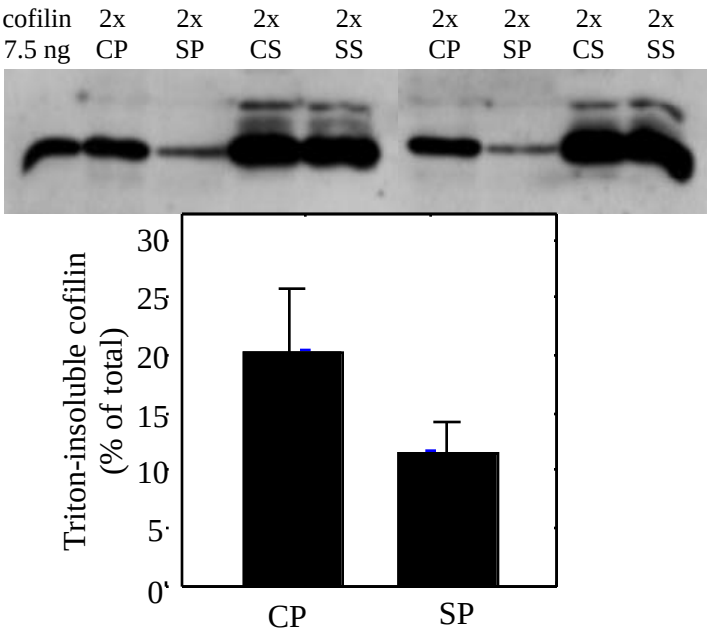

Fig. 4-3. *Cytoskeletal-associated cofilin levels in BAECs.* Confluent endothelial cells (CP) have twice as much cofilin associated with actin filaments as subconfluent cells (SP). CS = confluent supernatant; SS = subconfluent supernatant.

μM) [3]. By western blot the amount of cofilin in BAECs is estimated at ~1 μM, indicating that cofilin is not bound to ATP-actin in these cells. This implies that either more cofilin is dephosphorylated in confluent BAECs or that they have more ADP-F-actin subunits. Because the lifetime of actin filaments in confluent cells (~40 min) [1] is much longer than the lifetime of the ADP•Pi intermediate in ATP hydrolysis on filaments (~3 min) [15], it is reasonable to expect fewer ADP-bound F-actin subunits in these cells compared to the short-lived filaments (~7 minutes) in subconfluent cells [1]. Thus, the reduction in cofilin associated with F-actin is consistent with the reduction of ADP-actin content in filaments that should accompany more rapid actin filament turnover.

DISCUSSION

PAF studies reveal that endothelial cells alter their actin dynamics as they transition between motile states. Binding of ADF/cofilin to actin filaments could explain the observed relationships between endothelial cell speed, actin polymer fraction, and filament turnover. Since the slow rate of actin filament depolymerization *in vitro* is assumed the rate-limiting step in the actin cycle, cofilin would be expected to bind more F-actin subunits in highly motile subconfluent cells. However, subconfluent endothelial

cells have less cofilin associated with actin filaments than their slower moving confluent counterparts. One explanation is that the lifetime of actin filaments in slow-moving confluent cells greatly exceeds the ADP•Pi-bound F-actin subunit intermediate state, resulting in more ADP F-actin subunits in confluent endothelial cells, the preferred substrate for ADF/cofilin binding. The fact that more cofilin is associated with less dynamic actin in the slower phenotype implies that the regulation of cofilin binding to F-actin subunits by dephosphorylation is not an important mechanism in altering endothelial cell motility.

The cellular actin cycle is also regulated by proteins with mechanisms distinct from those attributed to ADF/cofilin (see review in Chapter I). Transition to the subconfluent phenotype coincides with a decrease in the average filament length, combined with an increase in the total number of actin filaments and uncapped barbed ends. Models that predict acceleration of treadmilling on linear [2, 16, 17] or branched [18] filament arrays cannot explain the observed changes in actin filament length, number, and polymer fraction. The most likely and efficient mechanism for generating more and smaller actin filaments is filament severing. The expression of gelsolin in fibroblasts increases cell speed in proportion to changes in actin dynamics. These experiments are consistent with a mechanism of severing-mediated actin filament disassembly, suggesting that gelsolin can indirectly regulate cofilin-induced depolymerization of actin filaments by creating new uncapped pointed ends. Severed filament barbed ends can also serve as nuclei for elongation, with or without intermediary capping by gelsolin. In this model, actin filament turnover and depolymerization correlate positively because of cofilin-mediated disassembly as described by others [19, 20], but exposure of actin filament pointed ends by severing, rather than dephosphorylation-induced translocation of cofilin to actin filaments, is responsible.

The observed changes in actin dynamics and filament properties may be explained by an alternative mechanism consisting of actin filament severing in the presence of constitutive accelerated actin filament turnover. This model is based on the relationship

between changes in actin filament length and turnover as endothelial cells change speed. From Eq. 2.13, the rate of change of actin filament length at steady state is dependent on the depolymerization kinetics at the actin filament pointed end. Because significant amounts of cofilin are associated with actin filaments in both BAEC motile phenotypes, if actin filament pointed ends are predominately uncapped, cofilin will accelerate depolymerization. However, since the turnover time of actin filaments is dependent on the average filament length (Eq. 2.15), longer actin filaments will take more time to depolymerize. In this way, at a constant rate of actin subunit loss from the pointed end, actin filament length is directly proportional to the lifetime of actin filaments. In support of this model, confluent endothelial cells were observed to have filaments that (on average) are ~7-fold longer than subconfluent cells, in almost a one-to-one correspondence with the measured 6-fold decrease in actin filament turnover times between these phenotypes. The small discrepancy between actin filament turnover and length may be explained by the capping of a small fraction of actin filament pointed ends, stabilizing these filaments against depolymerization. In this scheme, severing is required to shorten the length of actin filaments, thus reducing their lifetimes.

Finally, accelerated depolymerization coupled with *de novo* nucleation of actin filaments could lead to the observed changes in actin filament length and number as endothelial cells change their speed. This mechanism involves actin filament nucleation on the sides of pre-existing actin filaments by the Arp2/3 complex, creating a branched actin filament network [10]. In combination with accelerated depolymerization by ADF/cofilin, a branched treadmilling model has been postulated in which actin monomer assembles onto the barbed ends of actin filaments created by the Arp2/3 complex while ADF/cofilin accelerates depolymerization to recycle actin filament subunits into the monomer pool [18]. However, because of actin filament crosslinking by filamin and pointed end capping by the Arp2/3 complex, the filament length distribution would not shorten, and new actin filament ends would not be available for accelerated depolymerization. Thus, even in this model, severing is required to explain the vast changes in actin filament length and

number observed in endothelial cells moving at different speeds. Some investigators have proposed that ADF/cofilin has a weak severing activity [21-23], which may help to explain the slow rate of constitutive motility and actin dynamics in gelsolin-null fibroblasts. It is clear, however, that the addition of gelsolin to these fibroblasts increases cell speed, decreases the fraction of actin polymerized, and accelerates actin filament turnover, implicating the importance of gelsolin as an efficient severing mechanism in regulating endothelial cell motility.

REFERENCES

1. McGrath JL, Osborn EA, Tardy YS, Dewey CF, Jr., Hartwig JH: Regulation of the actin cycle in vivo by actin filament severing. Proc Natl Acad Sci U S A 2000; 97(12): 6532-6537.

2. Theriot JA: Accelerating on a treadmill: ADF/cofilin promotes rapid actin filament turnover in the dynamic cytoskeleton. J Cell Biol 1997; 136(6): 1165-8.

3. Carlier MF, Laurent V, Santolini J, et al.: Actin depolymerizing factor (ADF/cofilin) enhances the rate of filament turnover: implication in actin-based motility. J Cell Biol 1997; 136(6): 1307-22.

4. Kouyama T, Mihashi K: Fluorimetry study of N-(1-pyrenyl)iodoacetamide-labelled F-actin. Local structural change of actin protomer both on polymerization and on binding of heavy meromyosin. Eur J Biochem 1981; 114(1): 33-8.

5. Hartwig JH: Mechanisms of actin rearrangements mediating platelet activation. J Cell Biol 1992; 118(6): 1421-42.

6. Cooper JA: Effects of cytochalasin and phalloidin on actin. J Cell Biol 1987; 105(4): 1473-8.

7. Pollard TD: Rate constants for the reactions of ATP- and ADP-actin with the ends of actin filaments. J Cell Biol 1986; 103(6 Pt 2): 2747-54.

8. Bray D, Thomas C: Unpolymerized actin in fibroblasts and brain. J Mol Biol 1976; 105(4): 527-44.

9. Cano ML, Lauffenburger DA, Zigmond SH: Kinetic analysis of F-actin depolymerization in polymorphonuclear leukocyte lysates indicates that chemoattractant stimulation increases actin filament number without altering the filament length distribution. J Cell Biol 1991; 115(3): 677-87.

10. Mullins RD, Heuser JA, Pollard TD: The interaction of Arp2/3 complex with actin: nucleation, high affinity pointed end capping, and formation of branching networks of filaments. Proc Natl Acad Sci U S A 1998; 95(11): 6181-6.

11. Barbee KA, Davies PF, Lal R: Shear stress-induced reorganization of the surface topography of living endothelial cells imaged by atomic force microscopy. Circ Res 1994; 74(1): 163-71.

12. Arber S, Barbayannis FA, Hanser H, et al.: Regulation of actin dynamics through phosphorylation of cofilin by LIM- kinase. Nature 1998; 393(6687): 805-9.

13. Morgan TE, Lockerbie RO, Minamide LS, Browning MD, Bamburg JR: Isolation and characterization of a regulated form of actin depolymerizing factor. J Cell Biol 1993; 122(3): 623-33.

14. Ohta Y, Nishida E, Sakai H, Miyamoto E: Dephosphorylation of cofilin accompanies heat shock-induced nuclear accumulation of cofilin. J Biol Chem 1989; 264(27): 16143-8.

15. Carlier MF, Pantaloni D: Direct evidence for ADP-Pi-F-actin as the major intermediate in ATP- actin polymerization. Rate of dissociation of Pi from actin filaments. Biochemistry 1986; 25(24): 7789-92.

16. Small JV, Herzog M, Anderson K: Actin filament organization in the fish keratocyte lamellipodium. J Cell Biol 1995; 129(5): 1275-86.

17. Small JV: Microfilament-based motility in non-muscle cells. Curr Opin Cell Biol 1989; 1(1): 75-9.

18. Svitkina TM, Borisy GG: Arp2/3 complex and actin depolymerizing factor/cofilin in dendritic organization and treadmilling of actin filament array in lamellipodia. J Cell Biol 1999; 145(5): 1009-26.

19. Didry D, Carlier MF, Pantaloni D: Synergy between actin depolymerizing factor/cofilin and profilin in increasing actin filament turnover. J Biol Chem 1998; 273(40): 25602-11.

20. Carlier MF: Control of actin dynamics. Curr Opin Cell Biol 1998; 10(1): 45-51.

21. Du J, Frieden C: Kinetic studies on the effect of yeast cofilin on yeast actin polymerization. Biochemistry 1998; 37(38): 13276-84.

22. Maciver SK, Zot HG, Pollard TD: Characterization of actin filament severing by actophorin from Acanthamoeba castellanii. J Cell Biol 1991; 115(6): 1611-20.

23. Maciver SK, Pope BJ, Whytock S, Weeds AG: The effect of two actin depolymerizing factors (ADF/cofilins) on actin filament turnover: pH sensitivity of F-actin binding by human ADF, but not of Acanthamoeba actophorin. Eur J Biochem 1998; 256(2): 388-97.